AN ABSTRACT OF THE THESIS OF

Tin T. Nguyen for the degree of Master of Science in Electrical and Computer Engineering presented on June 29, 1993.

Title: Phosphor Development for Alternating-Current Thin-Film Electroluminescent Applications.

Redacted for Privacy

Abstract approved: _____

Dr. John F. Wager

The primary goal of this thesis is to describe a research program with the goal of exploring the potential of new phosphor materials for alternating-current thin-film electroluminescence (ACTFEL) applications.

ACTFEL devices employing the novel phosphor materials are fabricated with an additional thin layer of ZnS, which acts as a charge injection layer; such a charge injection layer is required because these materials either have a small density of interface states or these interface states are very deep. A $(Mg_{0.5}Zn_{0.5})SiN_2:Tb_4O_7$ ACTFEL device with a ZnS charge injection layer is fabricated. Charge transport across the phosphor is observed in this device. Green electroluminescence is also observed but it is quite dim; the maximum brightness is 0.53 fL at a voltage of 308 V and frequency of 1000 Hz. The green elctroluminescence is attributed to impact excitation of Tb by electrons transported across the $(Mg_{0.6}Zn_{0.4})SiN_2:Tb_4O_7$ layer and subsequent radiative emission. The as-deposited $(Mg_{0.5}Zn_{0.5})SiN_2:Tb_4O_7$ thin film is polycrystalline and

has a dielectric constant, resistivity, breakdown field, and optical bandgap of 11, $1.4x10^{13}$ ohm-cm, 2 MV/cm, and 4 eV, respectively.

A $(Mg_{0.6}Zn_{0.4})SiN_2:EuF_3$ ACTFEL device with a ZnS charge injection layer is also fabricated. Charge transport across the phosphor is also observed in this device. Red electroluminescence is observed but it is very dim; the maximum brightness is 0.045 fL at a voltage of 308 V and frequency of 1000 Hz. The red elctroluminescence is attributed to impact excitation of Eu and subsequent radiative emission. The as-deposited $(Mg_{0.6}Zn_{0.4})SiN_2:EuF_3$ thin film has the following electrical properties: dielectric constant of 11, resistivity of $1.2x10^{13}$ ohm-cm, and breakdown field of 2 MV/cm.

Phosphor Development for Alternating-Current Thin-Film Electroluminescent Applications

by

Tin T. Nguyen

A THESIS

submitted to

Oregon State University

in partial fulfillment of

the requirement for the

degree of

Master of Science

Completed June 29, 1993

Commencement June 1994

APPROVED:

Redacted for Privacy

Associate Professor of Electrical and Computer Engineering in charge of major

Redacted for Privacy

Head of Department of Electrical and Computer Engineering

Redacted for Privacy

Dean of Graduate School

Date thesis is presented June 29, 1993

typed by Tin T. Nguyen

Acknowledgments

I wish to express my sincere appreciation to Dr. John F. Wager for his guidance, encouragement, and patience during my graduate program. Special thanks are extended to Dr. D. Goodnick, Dr. B. Lee, and Dr. D. McIntyre for serving on my committee.

I would like to thanks Ming Ang for his encouragement and many useful discussions.

Thanks to Ahmad Abu-Dayal for his assistance in performing various measurements.

Special thanks to everyone in the Advance Technology groups at Planar Systems, especially Sey-Shing Sun, for supplying substrates, assisting in various experiments, and for technical support.

Thanks to Dr. Laura King for x-ray diffraction measurements.

This work was supported by the U.S. Army Research Office under contract D11L03-91G0242.

Table of Contents

Table of Contents, Continued

List of Figures

List of Figures, Continued

List of Tables

Phosphor Development for Alternating-Current Thin-Film Electroluminescent Applications

Chapter 1 - Introduction

Alternating-current thin-film electroluminescent (ACTFEL) devices are being employed for flat panel display (FPD) applications. Monochrome (yellow) electroluminescent FPDs are now in full production and multi-color (red and green) electroluminescent FPDs have just recently reached the market. The goal of most current ACTFEL research is to obtain full-color ACTFEL flat panel display.

To meet this goal, phosphors which emit red, green, and, blue (RGB) are needed. The main problem currently inhibiting the development of full-color ACTFEL flat panel displays is the inadequate brightness of the blue phosphor. Recently, multi-color, red-green ACTFEL displays have been released as a product. Sufficiently bright red and green pixels may be obtained by filtering the wide-band emission of the ZnS:Mn phosphor. Alternatively, bright green is obtained using a ZnS:Tb phosphor. However, the use of a filter adds complexity to the process and it also degrades the performance of other phosphors within the same panel. Therefore, it is desirable to develop a phosphor that efficiently emits red light.

The purpose of the work described in this thesis is to explore the potential of new materials for ACTFEL phosphor applications. Candidate phosphor materials are those that have properties which closely match that of ZnS:Mn, since this phosphor is very bright and efficient in emitting yellow-orange light. Thin film deposition is

accomplished via rf-sputtering. The sputtering system uses one and one quarter inch targets, which are prepared and pressed in-house. With this capability, new materials can be deposited and tested in a short amount of time.

The outline of the thesis is as follow. The following section presents the motivation for considering the ACTFEL phosphor materials studied in this thesis. Chapter 2 presents a review of ACTFEL device physics operation, and a description a the charge-voltage (Q_a-V_a), internal charge-phosphor field (Q-F_p), and capacitance-voltage (C-V) characterization techniques. Chapter 3 describes the characterization techniques used for thin film and ACTFEL device characterization using the new phosphor materials. The experimental results of ACTFEL devices fabricated using the newly developed phosphor materials are presented and discussed in Chapter 4. Finally, Chapter 5 includes conclusions and recommendations for future work.

1.1 ACTFEL Phosphor Candidates

The purpose of this section is to justify the choice of ACTFEL phosphor candidates studied in this thesis. Photoluminescence (PL) characterization is commonly used as an initial method for assessing the potential of new materials for ACTFEL phosphor applications. Potential ACTFEL phosphors are those that exhibit intense PL and also possess appropriate electrical properties such as appropriate breakdown field and low dielectric constant. It has been reported that $MgSiN_2$ exhibits blue PL with 40% quantum efficiency when

doped with Eu [1], therefore this material is a good candidate for an ACTFEL phosphor. Based on PL results obtained with $MgSiN_2$, some other ACTFEL phosphor candidate materials include $MgGeN_2$, $ZnSiN_2$, and $CaSiN_2$ [2]. It has been shown [2] that ACTFEL devices using $MgGeN_2$:EuF_3 as the phosphor exhibit red electroluminescence (EL) with a maximum brightness of 0.18 fL. On the other hand, $MgGeN_2$ films react with water [2], which excludes this material for use as an ACTFEL phosphor. Recently, $Al_{0.5}Ga_{0.5}N$ doped with rare-earth luminescence impurities was employed as an ACTFEL phosphor[3]. Based on these EL results, $AlInN_2$ could also be considered to be an ACTFEL phosphor candidate material.

Chapter 2 - Literature Review

2.1 History and Background

Electroluminescence (EL) is the non-thermal conversion of electrical energy into luminous energy. This phenomenon was first discovered in the early 1900's. However, not until the advent of thin-film technology has EL been usable for display technology. Since its discovery by the French Physicist Destriau [4] in 1936, there were many efforts to develop a usable and reliable display. It was not until 1974 when the first ACTFEL devices with long-term stability were introduced by Inoguchi et al. [5] The device of Inoguchi et al. was successful in maintaining a bright, stable luminescence for more than 10,000 hours using a double-insulator structure with ZnS:Mn as the phosphor. With this success and further understanding of this EL phenomenon, ACTFEL devices have matured from laboratory experiments to commercial production. 18-inch diagonal, monochrome (yellow) EL FPDs are now available in the commercial market place.

Much of todays research is focused on the development of the full-color EL displays and the development of new, efficient phosphors. The future of ACTFEL FPDs holds much promise since the ability to generate the three primary colors has been demonstrated in several laboratories [6-8]. The major problems that impede the development of full-color ACTFEL devices are having a blue phosphor with a sufficient luminescent intensity and the integration of a three-color system onto a single substrate. Two-color (red-

green) displays have been recently announed as a product[9]. A full-color display was recently demonstrated by Planar Systems[9].

2.2 ACTFEL Device Description

Preparation of ACTFEL devices is accomplished by employing one of the following process techniques: 1) sputtering, 2) evaporation, 3) metal-organic chemical vapor deposition (MOCVD), or 4) atomic layer epitaxy (ALE). The crystallinity of films prepared

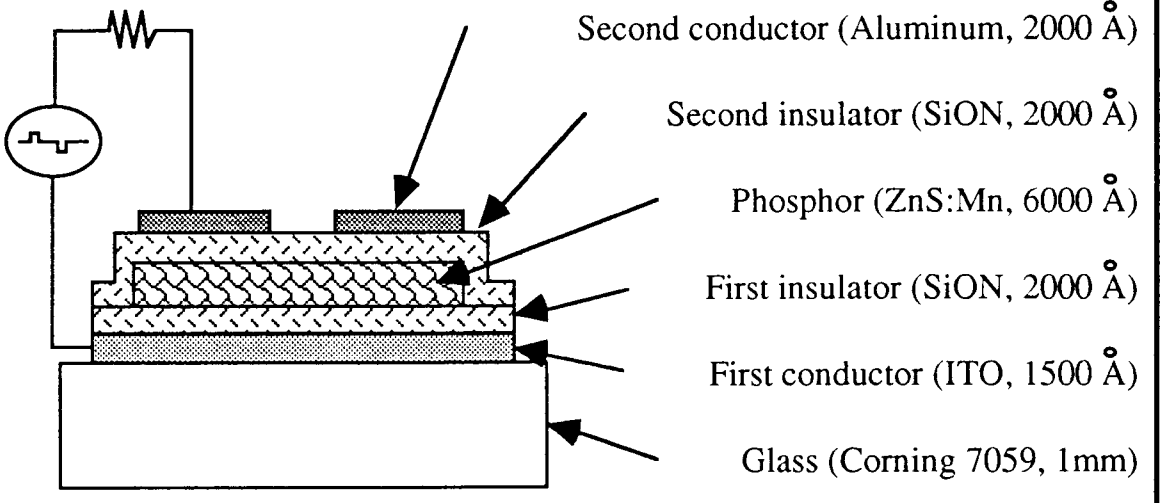

Figure 2-1. The structure of an ACTFEL device.

by sputtering or evaporation is usually improved by post-annealing the film at a very high temperature. Annealing can be accomplished using either a conventional thermal furnace or by employing rapid thermal anneal (RTA), where the annealing temperature can be as high as 1000° C.

The structure of an ACTFEL device is shown in Fig. 1. In the basic realization, the device consists of a stack of five layers of thin film. The stack is deposited on one side of a glass substrate about 1

mm thick. The first layer is a transparent electrical conductor, usually indium tin oxide (ITO), about 1500 angstroms thick. The second layer is an electrical insulator, such as silicon oxynitride (SiON), about 2000 angstroms thick. The third layer is a transparent phosphor layer, usually zinc sulfide doped with manganese (ZnS:Mn), about 6000 angstroms thick. The fourth layer is another electrical insulator, about 2000 angstroms thick. The fifth layer is a metallic electrical conductor, usually aluminum, about 2000 angstroms thick.

2.3 ACTFEL Phosphor

All phosphors consists of a host material and a light-emitting dopant called a luminescent impurity. Some of the desired properties of host material are: band-gap of approximately 3.0 eV or greater, a low dielectric constant, a breakdown field of approximately 1-2 MV/cm, maximum crystallinity, and the host cation of the phosphor to have a similar ionic radius and valence as the luminescent impurity that will replace it. A band gap of approximately 3 eV or greater is needed so that the entire visible light spectrum may be transmitted and the excited state of the luminescent impurity occurs well within the bandgap. Low dielectric constant ensures that most of the applied voltage drops across the phosphor instead of the insulator. This allows the ACTFEL device to operate at a lower voltage and this lowers the cost of the driving circuitry. A breakdown field of 1-2 MV/cm is found empirically to provide efficient ACTFEL operation. If the breakdown voltage is too small, the electrons are insufficiently heated as they drift across the

phosphor and do not efficiently excite luminescent impurities. If the breakdown voltage is too large, the device never turns on.

In order to be an efficient ACTFEL phosphor, the host material should have the best possible crystalline order. This allows electrons to efficiently gain sufficient kinetic energy from the electric field for impact excitation. Also, in order for the luminescent impurities to emit light efficiently, they should be incorporated in a substitutional lattice site, otherwise the excited center will lose its energy non-radiatively to the lattice. Note that a typical luminescent impurity dopant concentration in an ACTFEL phosphor is on the order of one percent. To obtain the required crystallinity at these high doping levels, both the geometrical size and the valence of the host cation should be matched with that of the dopant[10]. If there is a geometric mismatch, the probability of nonradiative recombination and atomic under device operation increases. If there is a valence mismatch, co-activator ions are needed for charge compensation. Since ACTFEL devices are operated under high fields (1-2 MV/cm), it is likely that these co-activator ions would migrate under device operation, consequently giving rise to device reliability problems.

2.4 ACTFEL Device Operation

Operation of the ACTFEL device involves the application of high voltage bipolar pulses to the two electrodes. The magnitude of the pulses is on the order of 150 to 200 V, which gives rise to an electric field in the phosphor layer of about 1.5 to 2 MV/cm, at which point the phosphor layer breaks down or starts conducting charge.

Therefore, the main function of the insulators is to prevent catastrophic breakdown of the device at the onset of phosphor breakdown. When the voltage reaches threshold, electrons begin to tunnel from interface states to the phosphor conduction band. The interface states are physically located at the interface region between the phosphor and the insulators, and are believed to reside approximately 0.6-0.8 eV below the conduction band minimum for an ACTFEL device with SiON insulators [11]. Injection of electrons from interface states is believed to be accomplished by one of three possible emission mechanisms: 1) thermal emission with Poole-Frenkel barrier lowering; 2) pure tunneling; or 3) phonon-assisted tunneling [11].

Once in the conduction band of the phosphor, the electrons gain kinetic energy from the electric field. These electrons, which have very high energies, can collide with luminescent impurities introduced into the phosphor. In the collision process, the electron can excite the outer electron of the luminescent impurity to an excited state. The excited electron of the luminescent impurity subsequently recombines radiatively and gives off the excitation energy as light. In the case of ZnS:Mn, the manganese emits wide-band yellow light with a peak intensity at 585 nm.

The emitted light reaches the viewer in various ways. Referring to Fig. 1, the light emitted in the phosphor layer can directly reach the viewer by propagating through the bottom insulator, through the ITO conductor, and through the glass substrate. It can also propagate through the top insulator, be reflected by the aluminum electrode,

propagate through the top insulator again, propagate through the phosphor, and eventually reach the viewer. Also, some of the light gets absorbed in the films and some is transmitted along the edge of the phosphor, due to the different indexes of refraction of the films. In order to obtain efficient transfer of light from the phosphor to the viewer, all the films, except the Al conductor, must be transparent.

2.5 ACTFEL Device Physics

2.5.1 Introduction

Recently, many papers on the operation and analysis of ACTFEL devices have been published [12-15]. In the following section, simplified energy band diagrams for various bias condition are examined in order to provide an understanding of how ACTFEL devices operate. The equations relating the physical quantities of interest are introduced subsequently. Following this section, various techniques used to characterize ACTFEL devices are presented with some brief description.

2.5.2 Energy Band Diagrams of ACTFEL Devices.

Figure 2-2 shows a simplified energy band diagram of an ACTFEL device. As can be seen, this energy band diagram represents an ACTFEL device under equilibrium, where the Fermi level is flat across the device. The Fermi level is assumed to lie near the midgap of the phosphor and the insulators. The bandgap of the ZnS phosphor is 3.68 eV and that of the SiON insulator is about 5.8 eV. The metallic conductor and the ITO (indium-tin-oxide), which is a

degenerate, n-type, transparent conductor, are shown on the left and right sides of the figure, respectively. Interface states between the phosphor and the insulator are represented by a series of horizontal bars. The nature of these interface states is not completely known. However, it is generally accepted that these are due to defects. The operation and performance of an ACTFEL device is believed to depend greatly on the density and energy depth of these interface states.

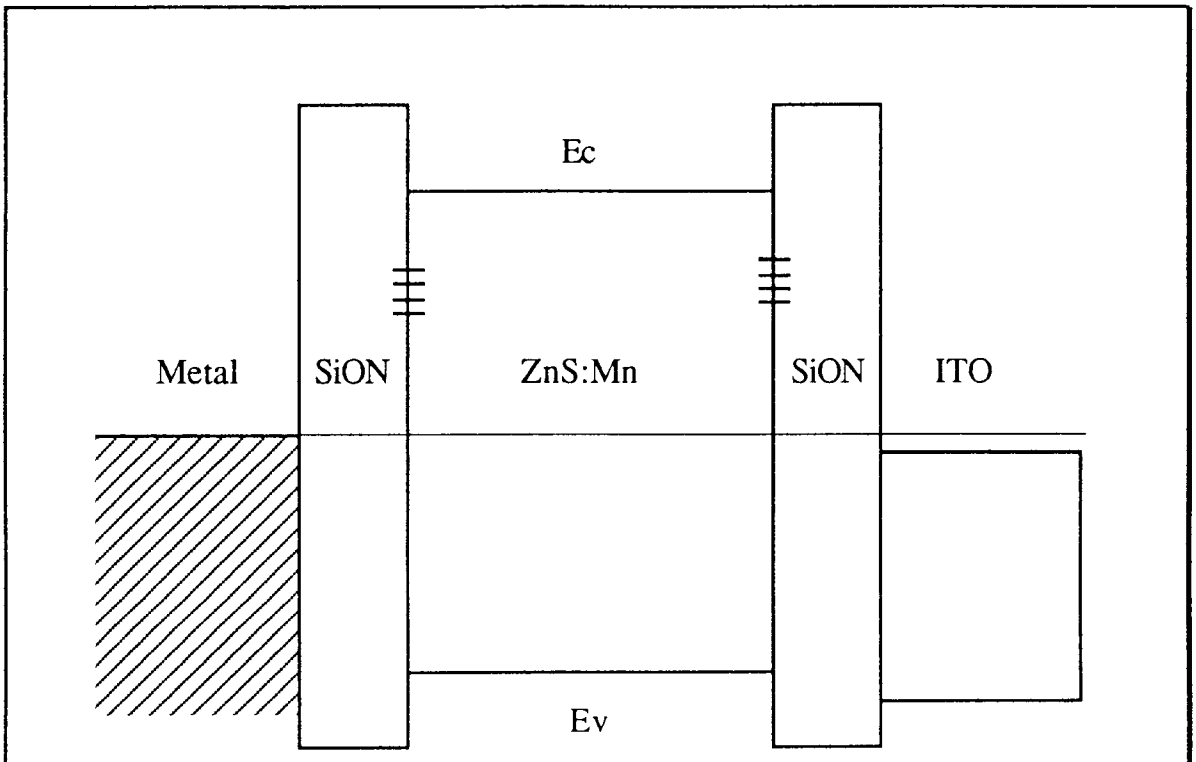

Figure 2-2. ACTFEL device energy band diagram in equilibrium.

Energy band diagrams of an ACTFEL device under normal operation, e.g. biased under an alternating voltage waveform, are shown in Fig. 2-3 through Fig. 2-6. When positive voltage is applied to the metallic conductor, the energy band diagram is as shown in

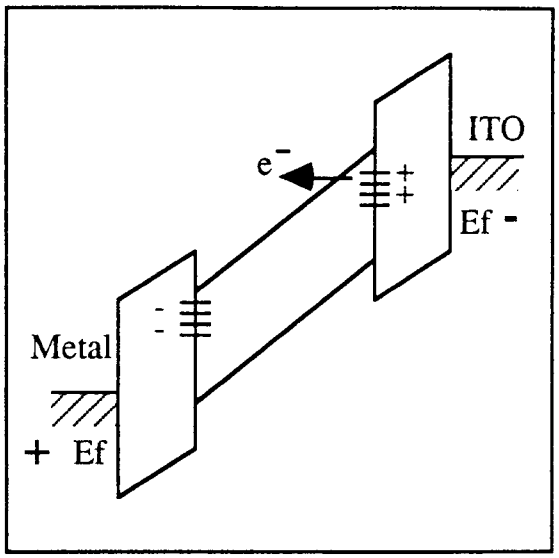

Figure 2-3. ACTFEL energy band diagram during positive bias.

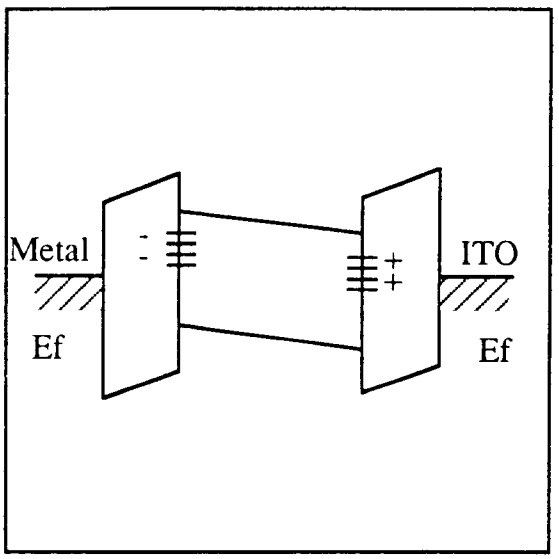

Figure 2-4. ACTFEL energy band diagram after positive bias.

Fig. 2-3. As can be seen, an electric field exists in the two layers of insulator and the phosphor. When a high enough field drops across the phosphor, electrons from the interface states on the ITO side tunnel-inject into the conduction band of the phosphor. Due to an abundance of these injected electrons, the phosphor electric field is effectively clamped. Once in the conduction band of the phosphor electrons accelerate toward the metal side, and are collected at the insulator-phosphor interface. Consequently, these trapped electrons, which now constitute polarization charge, set up an opposing electric potential. Once the applied bias returns to zero, the field in the phosphor remains due to trapped electrons at the interface, but the field direction is opposite to what it was under positive bias; this internal phosphor field at zero bias is called the polarization field. Figure 2-4 shows an energy diagram when the applied voltage goes to zero after the device is positively biased, and polarization charge

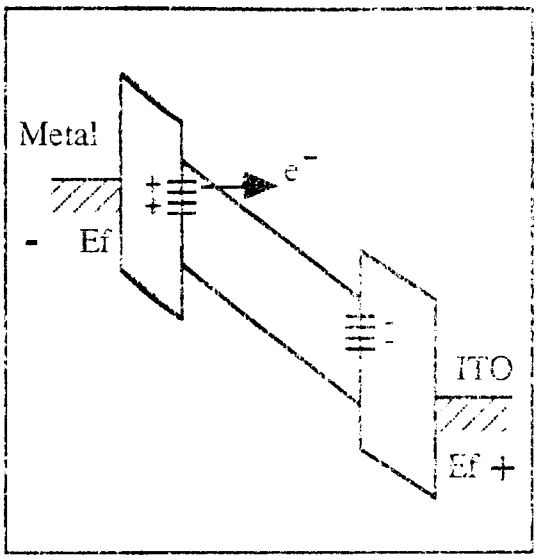

Figure 2-5. ACTFEL energy band diagram during negative bias.

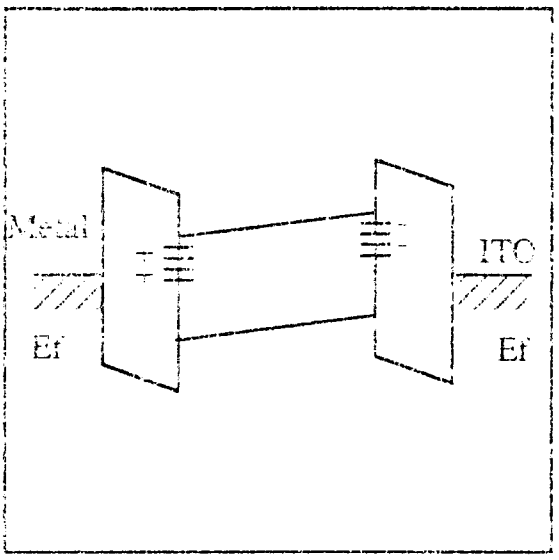

Figure 2-6. ACTFEL energy band diagram after negative bias.

has been transferred. During the zero bias period of the voltage, the polarization charge is assumed to remain constant. During the subsequent opposite polarity pulse the internal polarization field aids the external electric field in causing electrons to tunnel from interface states at a lower external bias magnitude than for the previous pulse. As in the case of the positive bias, after the voltage returns to zero, a polarization field exist within the phosphor. Energy band diagrams during and after the negative bias are shown in Fig. 2-5 and 2-6, respectively.

2.5.3 ACTFEL Electrostatics

To further understand the operation of an ACTFEL in detail, two physical quantities are of great interest, namely, the internal charge,

Q, and the phosphor electric field, F_p. In deriving for these two variables, begin with Gauss' law,

$$\oint_S D \bullet da = Q \qquad (2\text{-}1)$$

where **a** is a unit vector normal to an enclosed surface, and **D** is the electric displacement, which is

$$D = \varepsilon F \qquad (2\text{-}2)$$

where **F** is the electic field.

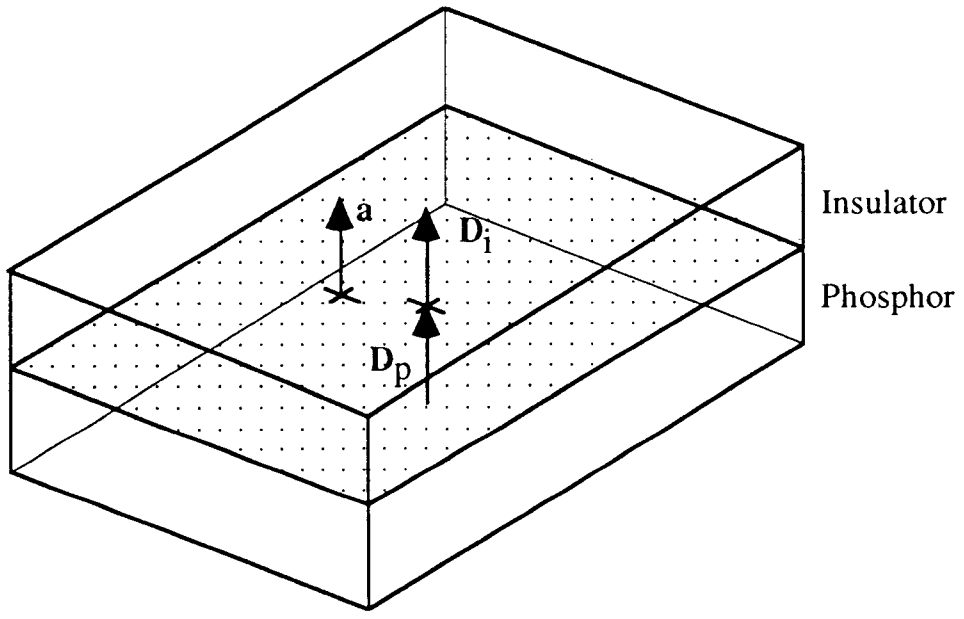

Figure 2-7. Gaussian surface at the interface between the insulator and the phosphor.

Figure 2-7 shows a Gaussian surface, which is a surface between the insulator and the phosphor of an ACTFEL device. After

evaluating the surface integral, Eqn. 2-1, the internal charge is given by,

$$Q = D_i - D_p = \varepsilon_i F_i - \varepsilon_p F_p \qquad (2\text{-}3)$$

where the subscript i and p refers to the insulator and the phosphor, respectively, and ε is the dielectric constant of the material.

From Eqn. 2-3, $\varepsilon_i F_i$ is a measurable quantity, now defined as Q_a. Q_a is the external charge per unit area as measured by a sense capacitor in series with the ACTFEL device and is given by [16]

$$Q_a = Q_{sense} = C_{sense} V_{sense} \qquad (2\text{-}4)$$

where C_{sense} is the value of the sense capacitor and V_{sense} is the voltage across it. Another measurable quantity is V_a, the applied voltage to the ACTFEL device. From Kirchoff's voltage law, the applied voltage is given by

$$V_a = d_i F_i + d_p F_p \qquad (2\text{-}5)$$

where d_i and d_p are the insulator and phosphor thicknesses, respectively. Solving Eqns. 2-3 through Eqn. 2-5 simultaneously, the internal charge is

$$Q = \left(\frac{C_i + C_p}{C_i}\right) Q_a - C_p V_a \qquad (2\text{-}6)$$

where C_i and C_p are the insulator and phosphor capacitance per unit area, respectively. Again, solving the above three equations simultaneously, the phosphor electric field is given by

$$F_p = \left(\frac{1}{d_p}\right)\left(V_a - \frac{Q_a}{C_i}\right). \qquad (2\text{-}7)$$

Equation 2-6 and 2.7 are used in the Q-F_p technique, which is described in the next section.

2.5.4 Analysis Techniques

The methods typically used to electrically characterize ACTFEL devices are charge-voltage (Q_a-V_a) [12], capacitance-voltage (C-V) [17], luminance-voltage (L-V), also called brightness-voltage (B-V), current-voltage (I-V), and internal charge-phosphor field (Q-F_p) [18]. The threshold voltage may be obtained from the first four methods, namely, Q_a-V_a, C-V, L-V, and I-V. The Q_a-V_a and C-V methods can be used to determine the capacitances before and after the phosphor breaks down, i.e. the total and insulator capacitances, respectively. The Q_a-V_a method may be used to determine the conduction and polarization charges. The Q-F_p and I-V methods provide information about the internal operation of the ACTFEL device. From the Q-F_p technique, the conduction, polarization, relaxation, and leakage charges may be determined as well as the steady-state field. The L-V technique is used to measure brightness. In this thesis, the C-V, Q-F_p, and Q_a-V_a techniques are used to characterize ACTFEL devices fabricated using the new phosphors; therefore, they are briefly reviewed below.

A Q_a-V_a plot is shown in Fig. 2-8. The curve is traced in a counter-clockwise direction as time progresses. A Q-F_p is also shown in Fig. 2-9. In this case, the curve is traced in a clockwise direction

as time progresses. A schematic for the driving waveform is shown in Fig. 2-10. As can be seen, the waveform is symmetric with alternating bipolar pulses of trapezoidal shape with 5 μs rise and fall times and a pulse width of 30 μs. The frequency of the waveform is 1 kHz. Various equivalent points of these three curves are labeled. The Q_a-V_a and Q-F_p plots shown are for an evaporated ZnS:Mn ACTFEL device.

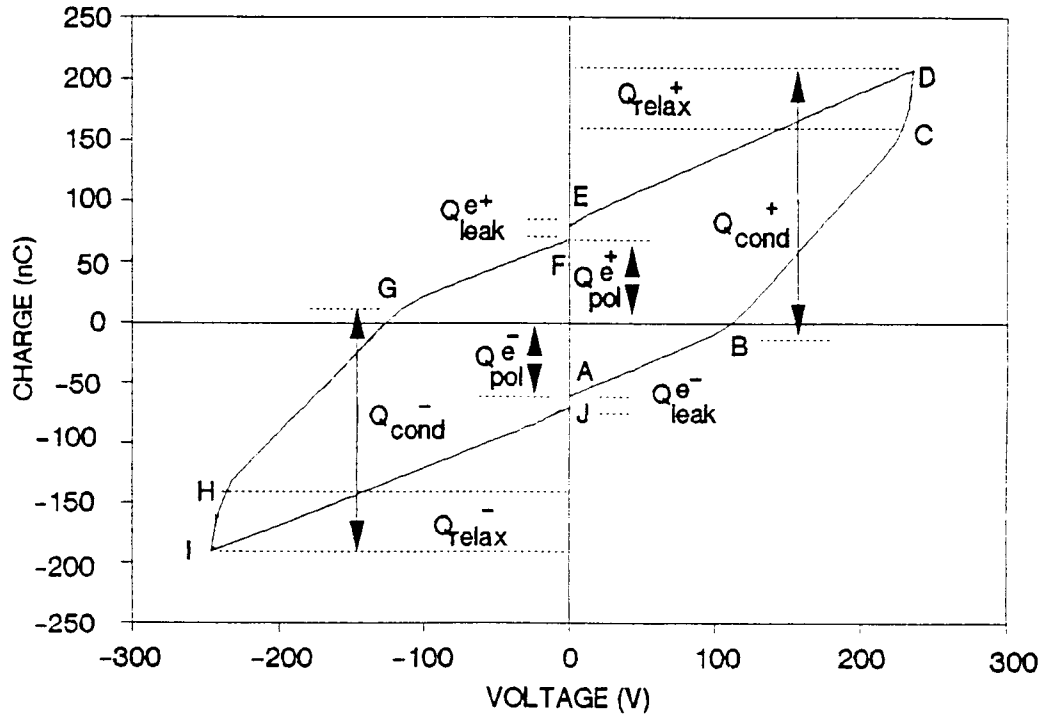

Figure 2-8. Q_a-V_a plot of a ZnS:Mn ACTFEL device. This plot is duplicated from reference 18.

From the Q_a-V_a and Q-F_p plots, it is seen that when the pulse voltage is zero, i.e. point A, the charge is not zero. This charge is due to electrons which remain trapped at interface states, this is the polarization charge left behind after the previously applied negative

pulse. As the applied voltage rises towards turn-on, i.e. A -> B, the Q_a-V_a curve rises linearly and the slope of the curve represents the total series capacitance of the phosphor and the insulators. This linear behavior indicates that the phosphor behaves like a capacitor in this range of voltage. Equivalently, the Q-F_p curve shows no change in the charge, even though the magnitude of the phosphor electric field increases.

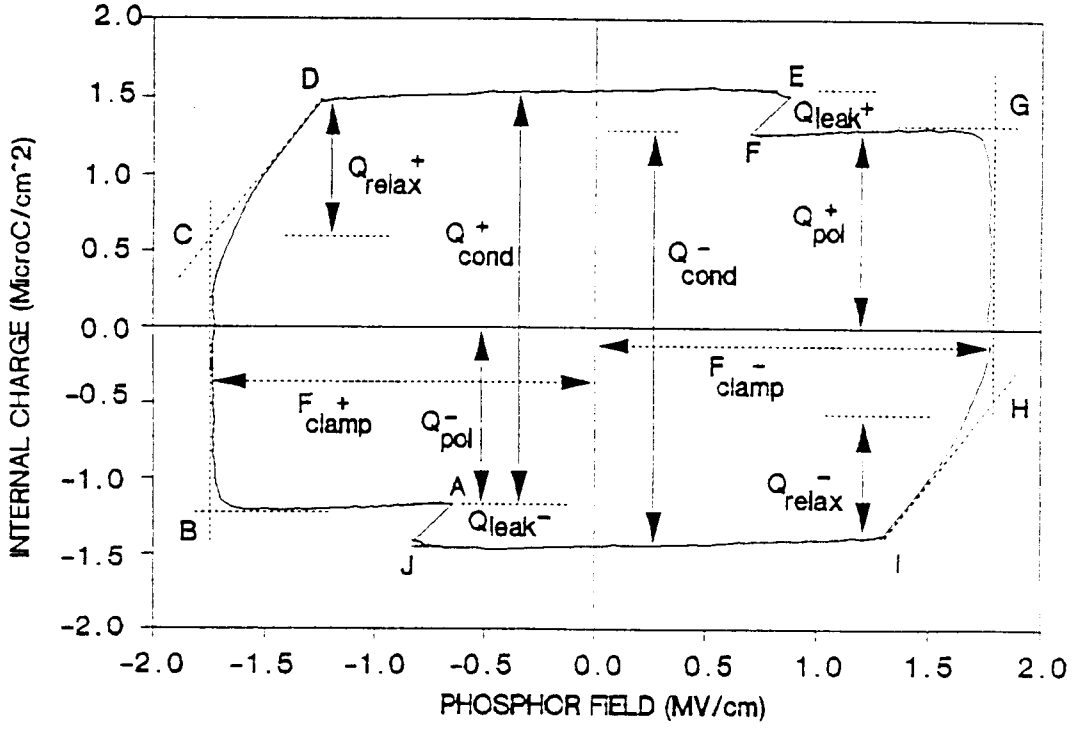

Figure 2-9. Q-F_p plot of a ZnS:Mn ACTFEL device. This plot is duplicated from reference 18.

As the applied voltage reaches the turn-on voltage, i.e. point B, electrons at interface states begin tunnel injection into the phosphor conduction band, leaving behind a positively charged interface. As

the voltage increases from turn-on to the maximum amplitude of the waveform (V_{max}) i.e. B-> C, the phosphor field, F_p, remains constant at F_{ss} (steady-state field) due to an abundance of injected electrons. If F_{ss} does not change with V_{max}, this behavior is referred to as field-clamping and the phosphor electric field is defined as F_{clamp}. The Q-F_p curve shows a vertical increase in the internal charge as electrons transit the phosphor. Equivalently, the Q_a-V_a curve is approximately linear from point B to C. The slope of the curve in this regime corresponds to the insulator capacitance if field-clamping occurs. Above turn-on, conduction occurs across the phosphor such that the phosphor capacitance is essentially shunted out of the circuit and any additional increase in the applied voltage drops across the insulators.

When the applied voltage reaches V_{max}, i.e. point C, electrons in the interface states continue to tunnel inject into the phosphor conduction band, transit the phosphor and get collected at the other interface. The Q-F_p curve shows an increase in the internal charge and the amplitude of the phosphor electric field decreases from point C to D. The charge transferred in this regime is refered to as relaxation charge [18] since F_p decays during the duration of the applied voltage waveform.

As the applied voltage decreases, i.e. D -> E, the Q_a-V_a curve shows that the capacitance is again the total series capacitance of the phosphor and the insulators. Also, the Q-F_p curve shows no change in the internal charge in this regime. As the applied voltage remains at zero, i.e. E -> F, some of the charge transferred during the previous

pulse transfers back to the original interface, which decreases the internal charge. The magnitude of the charge transferred in this regime is referred to as the leakage charge, which can be determined from both Q_a-V_a and Q-F_p curves. When the applied voltage reaches the onset of the next pulse, i.e. point F, again the internal charge is not zero due to the polarization charge. The remaining portions of the Q_a-V_a and Q-F_p curves, i.e. F -> A, is analogous to A -> F, except that it is associated with the opposite polarity pulse.

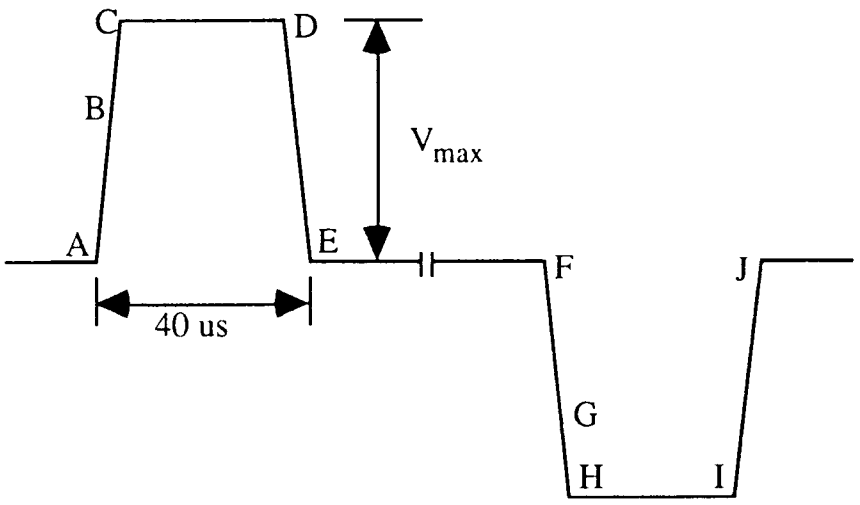

Figure 2-10. ACTFEL device driving waveform.

Precise values of the phosphor (C_p) and insulator (C_i) capacitances are needed in order to accurately calculate the internal charge (Q) from Eqn. 2-6 and the phosphor electric field (F_p) from Eqn. 2-7. These capacitances can be obtained from using two different methods. C_p and C_i can be calculated as parallel plate capacitors,

$$C = \varepsilon \frac{A}{d} \qquad (2\text{-}8)$$

where ε is the dielectric constant of the respective layer, **A** is the device area, and **d** is the thickness of the layer. This method is not very accurate since it is difficult to know the exact value of ε and d. A more accurate method is to extract C_p and C_i from the C-V plot of the same ACTFEL device. The capacitance is given by

$$C(v_a) = \frac{i(t)}{d[v_a(t)]/dt} \qquad (2\text{-}9)$$

where $v_a(t)$ is the voltage across the ACTFEL device and i(t) is given by

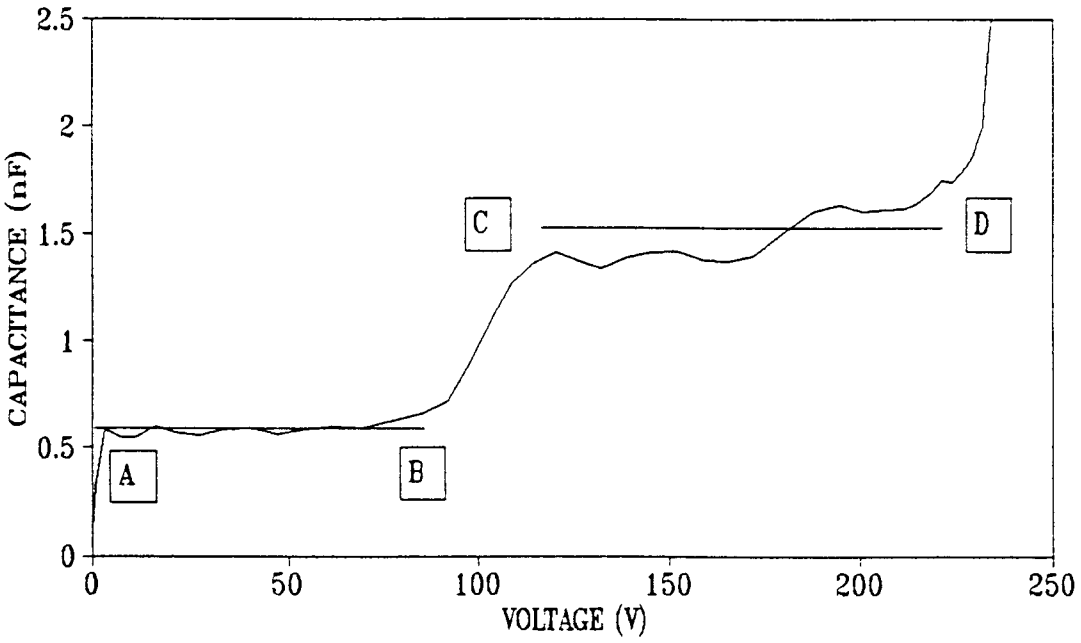

Figure 2-11. C-V plot of a ZnS:Mn ACTFEL device.

$$i(t) = \frac{v_3(t)}{R_c} \qquad (2\text{-}10)$$

where R_c is the current sense resistor and $v_3(t)$ is the voltage across R_c. The measurement set-up is shown in Fig. 3-3. A C-V plot of an ZnS:Mn ACTFEL device is shown in Fig. 2-11. From the C-V plot, it is seen that the total capacitance (C_t), C_p in series with C_i, corresponds to the region from point A to B. Point C to D corresponds to C_i, which is the capacitance due exclusively to the insulator layers after breakdown when the phosphor capacitance is shunted by conduction through the phosphor. The phosphor capacitance is then given by

$$C_p = \frac{C_t C_i}{C_i - C_t}. \qquad (2\text{-}11)$$

Chapter 3 - Experimental Techniques

This chapter describes the experimental techniques used for processing and characterizing the novel phosphor thin films and the ACTFEL devices. First, ACTFEL device deposition procedures and target preparation methods are presented. Second, phosphor thin films characterization techniques are discussed; this includes the measurement of resistivity, dielectric constant, optical bandgap, and crystal structure. Next, the techniques used for ACTFEL devices characterizion are presented. Also, the structure of the ACTFEL device and a simple ACTFEL device design procedure are include in this section.

3.1 Device Processing

3.1.1 ACTFEL Device Deposition Technique

Figure 2-1 shows that an ACTFEL device is comprised of several thin film layers. The thin films are deposited by the following deposition technologies. The ITO transparent conductor is pre-deposited onto a glass substrate from the vendor. The phosphor is deposited by sputtering. The insulator is deposited by sputtering or atomic layer epitaxy (ALE). The Al conductor is deposited by thermal evaporation. The ACTFEL devices fabricated for this thesis have an additional thin layer of ZnS between the insulator and the phosphor; this is called a charge injection layer, as in Section 3.3.1. This ZnS charge injection layer is deposited by either thermal evaporation or ALE. Note that the ALE layers are deposited at

Planar Systems. Also notice that the devices fabricated for the present study possess only one insulator layer, as discussed further in Section 3.3.1.

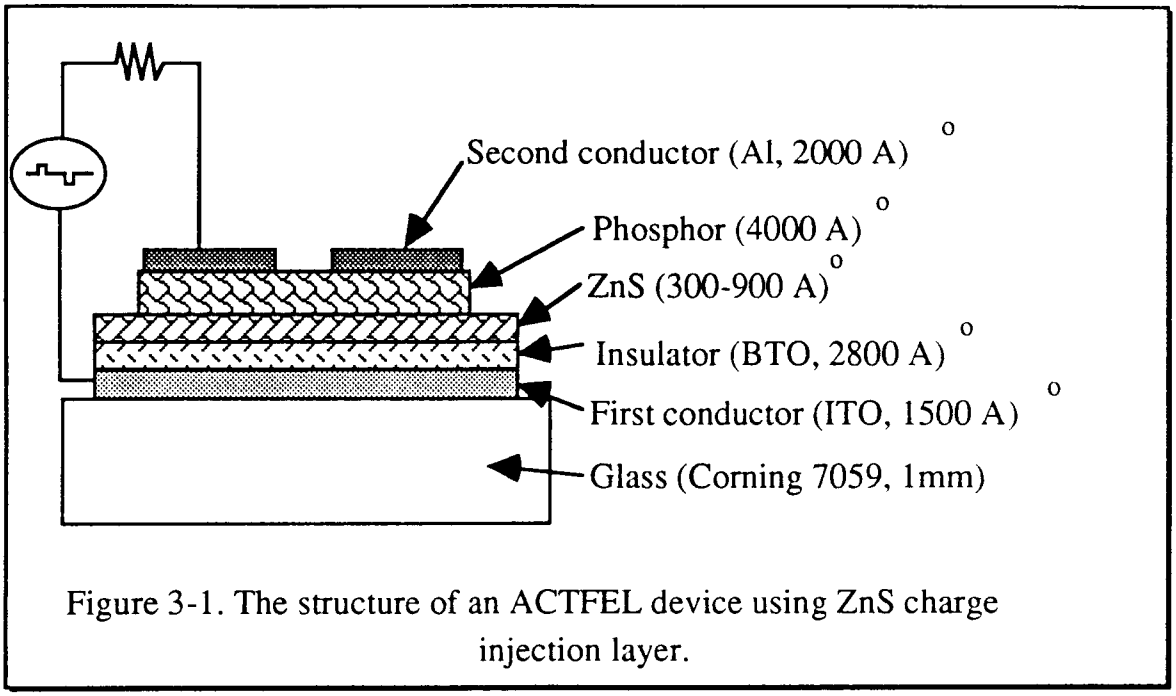

Figure 3-1. The structure of an ACTFEL device using ZnS charge injection layer.

3.1.2 Target Preparation

The phosphor targets used in this research are made in-house at OSU using a cold press. The target size is one and one quarter inches in diameter and one eight inch thick. The target is pressed from powder source materials, which are weighted to obtain the desired composition and mixed manually. The mixed powder is then placed into a stainless steel mold and pressed to a load of 15 tons using a hydraulic press. To prevent the target from falling apart, the mixed powder is pressed along with a piece of tin (Sn) foil, which is placed at the bottom of the mold. After pressing, the powder sticks to the tin foil. This tin foil provides strength to the formed target. It

also allows the formed target to be easily mounted to the magnetron sputtering gun.

3.2 Chacterization of Phosphor Thin Films

3.2.1 Device Structure

For resistivity and dielectric constant measurements, a phoshor film of about 2000 angstroms is deposited onto a glass substrate which was pre-deposited with an ITO conductor. Then, aluminum dots with an area of about 11.06×10^{-3} cm^2 and thickness of about 2000 angstroms are deposited on top of the phosphor film. The ITO and the aluminum dots serve as electrodes. For optical measurement, the phosphor film is deposited onto a fused silica substrate. Note, that a fused silica substrate is used instead of a glass substrate in order to avoid erroneous readings caused by optical absorbtion in the glass substrate. The equipment used for the electrical and optical measurements of phosphor thin films are listed in Table 3-1.

Measurement	Make	Model	Description
Resistivity	HP	4240B	pico-Ammeter/DC Voltage Source
Dielectric Constant	HP	4275B	Multi-frequency LCR Meter
Optical Band Gap	HP	8452A	Diode Array Spectrometer

Table 3-1. Equipment for electrical and optical measurements.

3.2.2 Electrical Properties

The resistivity is obtained from Ohm's law. By applying the voltage across the two electrodes and measuring the current, the resistivity is obtained as

$$\rho = \frac{A\ V}{I\ d} \qquad (3\text{-}1)$$

where A is the measured area, V is the applied voltage, I is the measured current, and d is the film thickness. The magnitude of the voltage is adjusted to obtain 1 MV/cm across the phosphor film. To avoid measuring transient effects, the current is measured after the voltage is applied for about 2 minutes.

The dielectric constant is obtained from

$$\varepsilon = \frac{C\ d}{A\ \varepsilon_o} \qquad (3\text{-}2)$$

where C is the measured capacitance, d is the film thickness, A is the area, and ε_o is the free space permittivity (8.854×10^{-4}). The capacitance is measured using a 10 kHz sinusoidal voltage of amplitude 0.25 V.

3.2.3 Optical Properties

The optical bandgap (E_o) is obtained from a Hewlett Packard transmittance measurement using a diode array spectrophotometer over a wavelength range of 190 nm to 820 nm. The absorption coefficient is related to the transmittance by

$$\alpha \approx \frac{A}{d} = \frac{-\ln(T)}{d} \qquad (3\text{-}3)$$

where A is the area, T is the transmittance, and d is the film thickness. From the absorbtion coefficient, E_o can be obtained from a Tauc plot [20] which is a plot of

$$\sqrt{\alpha E} = \sqrt{B}\left(E - E_o\right) \text{ versus } E, \qquad (3\text{-}4)$$

where E_o is equal to the x-intercept.

3.2.4 Structural Characterization

X-ray diffraction is employed to obtain the crystalline nature of the phosphor film. X-ray diffraction spectrums of the phosphor films are obtained from a Siemens, model # D5000, x-ray diffraction measurement system. To better resemble the phosphor film used in the ACTFEL device, the tested film is deposited on to a pre-deposited ITO glass substrate.

3.3 Design and Characterization of ACTFEL Devices

3.3.1 ACTFEL Device Structure

In order for an ACTFEL device to effictively emit light, conduction charge within the phorphor is required. Because the novel phosphors studied either have a small density of interface states or these interface states are very deep, a negligible amount of conduction charge is found to flow when ACTFEL devices are fabricated without a charge injection layer. To overcome this problem, a thin ZnS charge injection layer is placed between the

insulator and the phosphor. Such ACTFEL devices with ZnS charge injection layers show very efficient charge injection from interface states into the conduction band of the ZnS layer. ACTFEL devices using ZnS charge injection layers are believed to operate as follows: At a sufficiently high applied voltage, electron injection from the insulator-ZnS interface into the ZnS conduction band occurs. These carriers are either trapped at the ZnS-phosphor interface if the ZnS-phosphor conduction band discontinuity is sufficiently large or they surmount this discontinuity and are injected into the phosphor conduction band. As the applied voltage is increased further, electrons trapped at the ZnS-phosphor interface can also be injected into the phosphor conduction band. Once in the phosphor conduction band, these carriers transverse the phosphor and are collected at the other side of the phosphor interface. The structure of an ACTFEL device using a ZnS charge injection layer is shown in Fig. 3-1. Notice that only one insulator layer is used. The primary reason for using only one insulator is the ease of fabrication. Also, $BaTa_2O_6$ (BTO) is used instead of SiON because BTO has a higher dielectric constant (ε=18 F_{bd}=2.5 MV/cm).

3.3.2 ACTFEL Device Design

In order to effectively design an ACTFEL device, it is necessary to specify the thickness of the insulator and phosphor. In this section, a simple ACTFEL device design procedure is presented. This ACTFEL device design procedure builds on that formulated by Ang[2].

In the design procedure presented herein, it is assumed that there is no leakage nor relaxation charge in the phosphor layer. Moreover, it is also assumed that field-clamping occurs in the phosphor layer (i.e. $F_p=F_{clamp}$) and the phosphor breaks down totally (i.e. most of the trapped carriers at the ZnS-phosphor interface are injected into the phosphor conduction band and traverse the phosphor). The ideal Q-F_p and Q_a-V_a plots for this ACTFEL device are shown in Fig. 3-2.

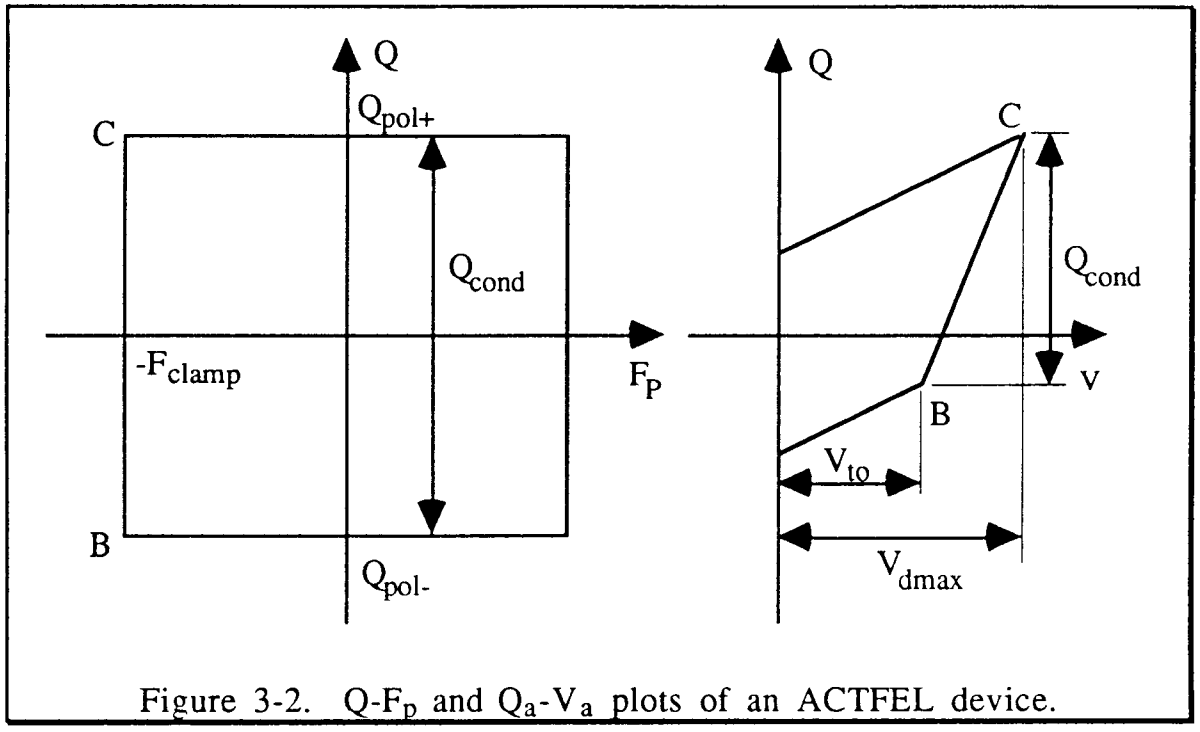

Figure 3-2. Q-F_p and Q_a-V_a plots of an ACTFEL device.

The electrostatic boundary condition at point C in Fig. 3-2 requires that

$$Q_{pol+} = \varepsilon_i F_{i,C} - \varepsilon_p F_{clamp} \qquad (3\text{-}4)$$

where $F_{i,C}$ is the insulator electric field and Q_{pol+} is the polarization charge at point C. Also, ε_i and ε_p are the dielectric constants of the insulator and phosphor respectively. Note that in practice, there is an upper limit beyond which the insulator breakdown occurs and the ACTFEL device is permanently destroyed (i.e. the ACTFEL device "burns out"); denote this maximum insulator field as F_{bd}. From Eqn. 3-4, the following condition must be satisfied in order to operate the ACTFEL device below "burn out".

$$F_{bd} > \frac{\varepsilon_p}{\varepsilon_i} F_{clamp} + \frac{Q_{pol+}}{\varepsilon_i} . \qquad (3\text{-}5)$$

To turn on the ACTFEL device, i.e. to have a non-zero Q_{pol+}, Eqn. 3-5 indicates that the following condition must be satisfied,

$$F_{bd} > \frac{\varepsilon_p}{\varepsilon_i} F_{clamp} . \qquad (3\text{-}6)$$

If Eqn. 3-6 is not satisfied, then the ACTFEL device burns out before it can be turned on, independent of the phosphor or insulator thickness. Equation 3-6 underscores the importance of using an insulator with a large dielectric constant and/or a high breakdown field, especially if the phosphor has a large dielectric constant and/or a high clamping field.

Once the type of phosphor and insulator have been chosen, so that Eqn. 3-6 is satisfied, the next step is to calculate the thickness of these layers (i.e. d_i and d_p). Note that d_i is the total insulator thickness. In order to calculate the thickness, two variables must be first specified. The first variable is the maximum voltage of the

waveform driver, V_{dmax}; this is the maximum amplitude that can be provided by the waveform driver for testing the ACTFEL device. The second variable to be specified is the ACTFEL device turn-on voltage, V_{to}, the external voltage at which electron injection from the interface occurs. Note that $(V_{dmax}-V_{to})$ is the operating voltage range of the designed ACTFEL device.

From the symmetry of the Q-F_p plot shown in Fig. 3-2, Q_{pol+} and Q_{pol-} are equal in magnitude and are given by

$$Q_{pol+} = -Q_{pol} = \frac{1}{2}Q_{cond} = \frac{\varepsilon_i}{2d_i}\left(V_{dmax} - V_{to}\right). \qquad (3\text{-}7)$$

By substituting Eqn. 3-7 into Eqn. 3-5, the minimum insulator thickness required in order to prevent ACTFEL device burn out is given by

$$d_i \geq \frac{V_{dmax} - V_{to}}{2\left(F_{bd} - \frac{\varepsilon_p}{\varepsilon_i}F_{clamp}\right)}. \qquad (3\text{-}8)$$

Note that the required condition given by Eqn. 3-6, i.e. $F_{bd} > \varepsilon_p F_{clamp}/\varepsilon_i$, is also a required condition for Eqn. 3-8 in order to have a meaningful (positive) insulator thickness.

The relationship between V_{to} and the insulator, phosphor, and ZnS layer thickness is given by

$$V_{to} = d_i F_{i,B} + d_z F_{z,B} + d_p F_{clamp} \qquad (3\text{-}9)$$

where $F_{i,B}$ is the insulator electric field and $F_{z,B}$ is the ZnS layer electric field at point B. Also, d_z is the ZnS layer thickness. From Gauss' law, the relationship between $F_{z,B}$ and F_{clamp} is given by

$$F_{z,B} = \frac{Q_{z\text{-}p}}{\varepsilon_z} + \frac{\varepsilon_p}{\varepsilon_z} F_{clamp} \qquad (3\text{-}10)$$

where $Q_{z\text{-}p}$ is the charge at the ZnS-phosphor interface and ε_z is dielectric constant of the ZnS. From the electrostatic boundary condition at point B, the insulator electric field, $F_{i,B}$ is given by

$$F_{i,B} = \frac{Q_{pol\text{-}}}{\varepsilon_i} + \frac{\varepsilon_p}{\varepsilon_i} F_{clamp} \cdot \qquad (3\text{-}11)$$

Solving Eqns. 3-7, 3-9, 3-10, and 3-11 simultaneously, the phosphor thickness is

$$d_p = \frac{V_{to} + V_{dmax}}{2F_{clamp}} - \left(\frac{\varepsilon_p}{\varepsilon_i} d_i + \frac{\varepsilon_p}{\varepsilon_z} d_z + \frac{Q_{z\text{-}p}}{\varepsilon_z} \right). \qquad (3\text{-}12)$$

From the previous assumption that the phosphor breaks down totally, i.e. there is no charge at the ZnS-phosphor interface, $Q_{z\text{-}p}$ is zero and the phosphor thickness is now given by

$$d_p = \frac{V_{to} + V_{dmax}}{2F_{clamp}} - \left(\frac{\varepsilon_p}{\varepsilon_i} d_i + \frac{\varepsilon_p}{\varepsilon_z} d_z \right). \qquad (3\text{-}13)$$

When designing an ACTFEL device using a new phosphor and insulator combination, ε_p, V_{bd}, and ε_p can be measured experimentally from single-layer phosphor and insulator thin films. However, F_{clamp} can only be determined by fabricating and testing an ACTFEL device. For first-cut design of an ACTFEL device using a new phosphor, a simple guess must do for F_{clamp}. The dielectric

constant (ε_z) and thickness (d_z) of the ZnS are usually known values in the ACTFEL design procedure.

An example of ACTFEL device design parameters is given in Table 3-2. From these known parameters and Eqn. 3-8, d_i > 4000 Angstroms. Let d_i = 3846 Angstroms, d_p = 9292 Angstroms. Thus, in the ACTFEL design procedure, the insulator and phosphor material are first chosen so that Eqn. 3-6 is satisfied; then d_i is chosen based on Eqn. 3-8. Finally, d_p is calculated using Eqn. 3-13 and the chosen value of d_i.

Variable	Value	Variable	Value
ε_p	15	V_{dmax}	300 V
ε_z	5	F_{clamp}	2 MV/cm
ε_i	25	d_z	300 A°
F_{bd}	2.5 MV/cm	d_i	3846 A°
V_{to}	200 V	d_p	9292 A°

Table 3-2. An example of ACTFEL design parameters.

There are three possible outcomes of the measured response for an ACTFEL device fabricated using the dimensions obtained from the first-cut ACTFEL device design procedure: the device operates as expected, the device does not turn on, or the device burns out. In the case that the device burns out, Eqn. 3-5 indicates that either Q_{pol+} is too large or the insulator dielectric constant is too small. To solve the problem of low insulator dielectric constant, an insulator

Description	Make	Model
High voltage power supply	Kikusui Electronics Corp.	PAB350-0.2
High voltage amplifier	OSU	-
Waveform generator	Wavetek	275
Digitizing Oscilloscope	Tektronix, Inc.	7854
Photometer	Tektronix, Inc.	J6523
Photo-multiplier tube	Product for Research, Inc.	7102/117
Temperature controller	Product for Research, Inc.	-
High voltage power supply	Pacific Precision Instr.	204
Monochromater	Jarrel-Ash	128A
Lock-in amplifier	EG&G Princeton Applied Research	128A

Table 3-3. List of equipment used for ACTFEL device characterization.

with a higher dielectric constant should be used. If Q_{pol+} is too large, it could be reduced by increasing the insulator thickness, as indicated by Eqn. 3-7. In the case that the device does not turn on when V_{dmax} is reached, Eqn. 3-9 indicates that the actual clamping field must be higher than that estimated. In this case, the phosphor thickness must be reduced, as indicated by Eqn. 3-13. Thus in a few design iterations, the value of the clamping field may be more accurately estimated and a better design for the ACTFEL device can be obtained.

3.3.3 Equipments

Table 3-3 lists the equipments used in characterizing the ACTFEL devices fabricated using the new phosphors. All of the measurements are accomplished using bipolar pulses with a 1 kHz frequency, 30 μs pulse width, and 5 μs rise and fall times. The waveform is shown in Fig. 2-10. A 0.5-2 KΩ resistor is connected in

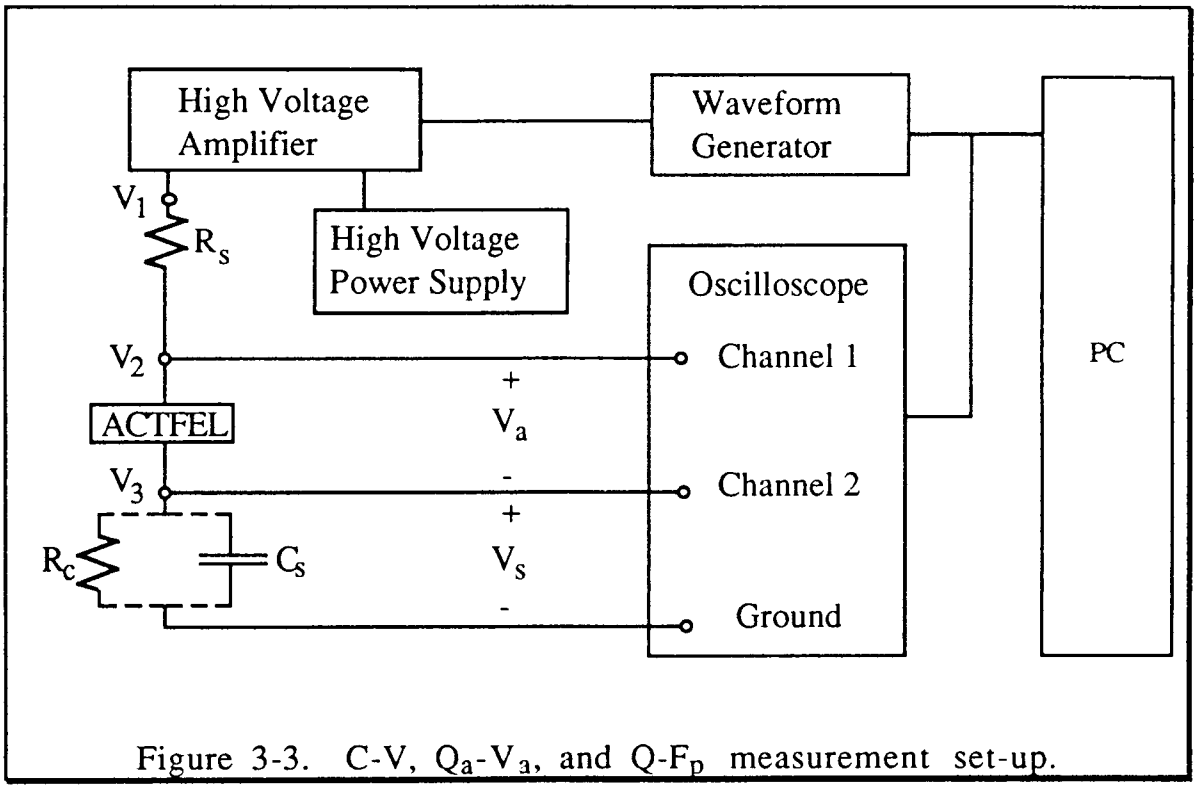

Figure 3-3. C-V, Q_a-V_a, and Q-F_p measurement set-up.

series with the ACTFEL device to prevent device burn out. This series resistor also protects the waveform driver when an ACTFEL device burns out.

3.3.4 C-V, Q_a-V_a, and Q-F_p Measurements

The C-V, Q_a-V_a, and Q-F_p experimental setup is shown in Fig. 3-3. Figure 3-3 shows that the ACTFEL device is connected in series with a resistor (R_s) and either a current sense resistor (R_c) or a sense capacitor (C_s); R_c is used for the C-V measurement while C_s is used for Q_a-V_a and Q-F_p measurements. Again, R_s is used as a current limiter. C_s integrates charge which flows into the ACTFEL device terminal. In order to have most of the voltage drop across the ACTFEL device, the value of C_s should be large (e.g. 100 times the ACTFEL devices total capacitance). R_c is used to monitor the current flow in the ACTFEL device. To avoid too much voltage drop across R_c, the value of R_c should be small (e.g. 10 Ohms). The voltage drop across the ACTFEL device (v_2-v_3) and across the current sense resistor or sense capacitor (v_3) are acquired using a digital oscilloscope. The waveforms are then stored and processed using a computer. A C-V plot can be obtained from Eqn. 2-9. A Q_a-V_a plot can be obtained from Eqns. 2-4 and 2-5. A Q-F_p plot can be obtained from Eqns. 2-6 and 2-7.

3.3.5 Optical Measurements

A set-up for the brightness-voltage (B-V) measurement is shown in Fig. 3-4. A photometer is placed in front of the ACTFEL device to monitor the output brightness. The voltage and brightness are recorded manually. Due to the low light output, the measurement is taken in a very dark room.

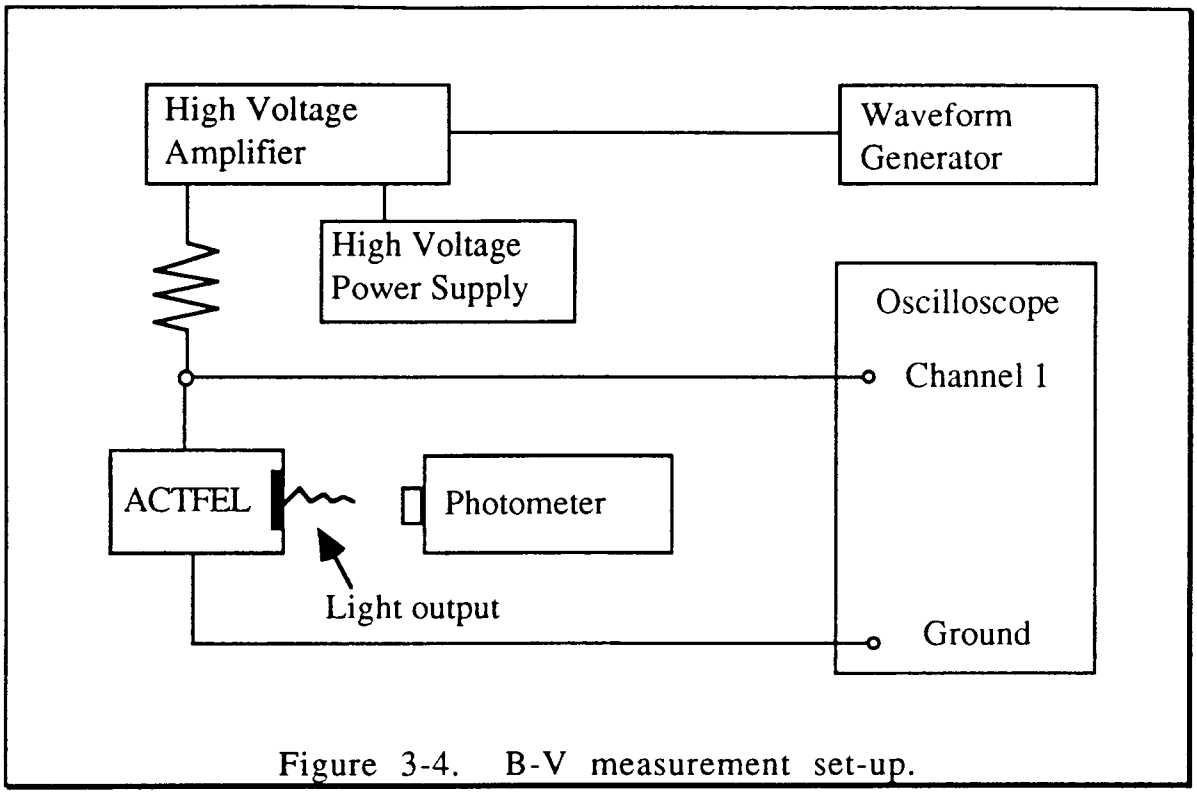

Figure 3-4. B-V measurement set-up.

The electroluminescence spectrum measurement set-up is shown in Fig. 3-5. Again, because the light is very dim, a lock-in amplifier is used. Although the waveform frequency is 1 kHz, the reference frequency of the lock-in amplifier is set to 2 kHz, because the light is emitted for both positive and negative pulses. All the data are recorded via the computer. The measurement parameters are given in Table 3-4.

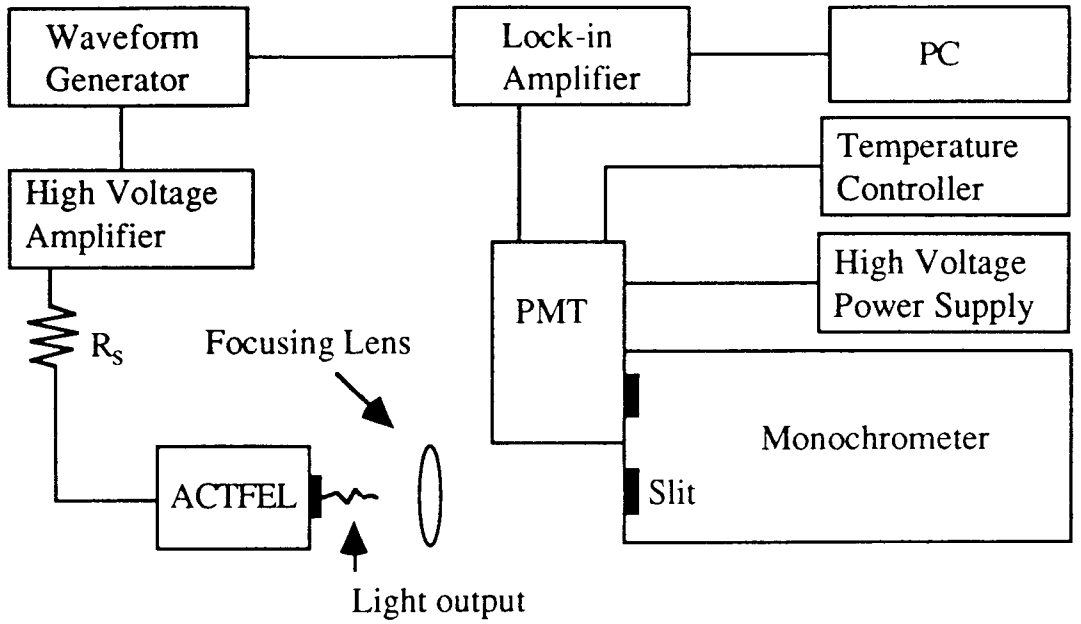

Figure 3-5. Electroluminescence spectrum measurement set-up.

Setting	Value	Setting	Value
PMT Voltage	1020	Lock-in Amp. Sensitivity	2.5 us
PMT Temperature	-90 ℃	Lock-in Amp. Time Constant	10 s
Slit	2.4 mm	Lock-in Amp. Frequency	2 kHz
Scan Speed	125 Å/min	Pulse Amplitude	270 V
Rs	1 kOhm	Pulse Frequency	1 kHz

Table 3-4. Electroluminescence spectrum measurement set-up parameters.

Chapter 4 - Experimental Results

This chapter presents experimental results obtained from characterization of the novel phosphor thin films and ACTFEL devices. First, a general discussion of the characterization of all the phosphor thin films and ACTFEL devices studied is presented. The phosphor thin films are characterized electrically and optically by evaluating the resistivity, dielectric constant, breakdown field, and optical bandgap. ACTFEL device characterization is accomplished by C-V, Q_a-V_a, Q-F_p, and B-V analysis and by measuring the elctroluminescence spectrum. The results of the more thorough characterization of the most promising phosphor material studied, which is sputtered from a $(Mg_{0.5}Zn_{0.5})Si_3N_4$:$Tb_4O_7$ target, is presented next. In addition to all of the thin film and ACTFEL device characterization techniques mentioned above, this phosphor thin film is also characterized x-ray diffraction to assess the crystalline nature of the film.

4.1 Target Compositions

The target compositions used in depositing the phosphor thin films studied in this thesis are listed in Table 4-1. The processing parameters used to deposit the phosphor thin films are presented in Table 4-2. Notice, no attempt is made to optimize the process.

Target	Chemical	Purity (%)	Mesh	Mole (at. %)
AlIn:Eu2O3	Al	99.5	325	49.5
	In	99.99	150	49.5
	Eu2O3	99.9	-	1 (EuO1.5)
MgSi3N4:Eu2O3	Mg	99.6	325	49.5
	Si3N4	99.9	-	49.5 (siN1.33)
	Eu2O3	99.9	-	1 (EuO1.5)
ZnSi3N4:Eu2O3	Zn	97.5	-	49.5
	Si3N4	99.9	-	49.5 (SiN1.33)
	Eu2O3	99.9	-	1 (EuO1.5)
Ca3N2Si3N4:Eu2O3	Ca3N2	99	-	49.5
	Si3N4	99.9	-	49.5 (SiN1.33)
	Eu2O3	99.9	-	1 (EuO1.5)
MgZn0.5Ge0.5:Eu2O3	Mg	99.6	325	49.5
	Zn	97.5	-	24.75
	Ge	99.999	100	24.75
	Eu2O3	99.9	-	1 (EuO1.5)
Mg0.8Zn0.8Si3N4:EuF3	Mg	99.6	325	39.6
	Zn	97.5	-	9.9
	Si3N4	99.9	-	49.5 (SiN1.33)
	EuF3	99.9	-	1
Mg0.6Zn0.4Si3N4:EuF3	Mg	99.6	325	29.7
	Zn	97.5	-	19.8
	Si3N4	99.9	-	49.5 (SiN1.33)
	EuF3	99.9	-	1
Mg0.5Zn0.5Si3N4:Tb4O7	Mg	99.6	325	24.75
	Zn	97.5	-	24.75
	Si3N4	99.9	-	49.5 (SiN1.33)
	Tb4O7	99.9	-	1 (TbO1.75)

Table 4-1. Target source materials.

Target	Ar/N2 (sccm/sccm)	Power (Watts)	Pressure (mTorr)	Rate Å / min
AlIn:Eu2O3	80/20	70	20	95
MgSi3N4:Eu2O3	80/20	70	20	73
ZnSi3N4:Eu2O3	80/20	70	20	-
MgGe0.5(Si3N4)0.5:Eu2O3	90/10	70	20	102
Mg0.8Zn0.2Si3N4:EuF3	90/10	70	20	76
Mg0.6Zn0.4Si3N4:EuF3	90/10	70	20	60
Mg0.5Zn0.5Si3N4:Tb4O7	90/10	70	20	73

Table 4-2. Processing parameters used for phosphor deposition.

4.2 Phosphor Materials Evaluation

4.2.1 $AlInN_2$:Eu_2O_3

The first phosphor material studied is $AlInN_2$:Eu_2O_3. The phosphor film has the following electrical properties: dielectric constant of 12.5, resistivity at 1 MV/cm of 2.2 x 10^9 ohm-cm, and breakdown field of 1.5 MV/cm. The $AlInN_2$:Eu_2O_3 ACTFEL device is fabricated using the device structure shown in Fig. 3-1 but without the ZnS charge injection layer. A Q-F_p plot of this device is shown in Fig. 4-1. The Q-F_p plot is measured at 173 volts using the waveform shown in Fig. 2-10. From the Q-F_p plot, it is seen that about 8 microC/cm^2 of charge conducts across the phosphor; conduction is initiated at a very low phosphor field and the device is very leaky. Low-field conduction, i.e. too low for efficient impact excitation and large leakage charge are undesirable characteristics for an ACTFEL

device. No luminescence is observed at 180 volts, the maximum voltage of operation. This is presumably due to the low-field conduction.

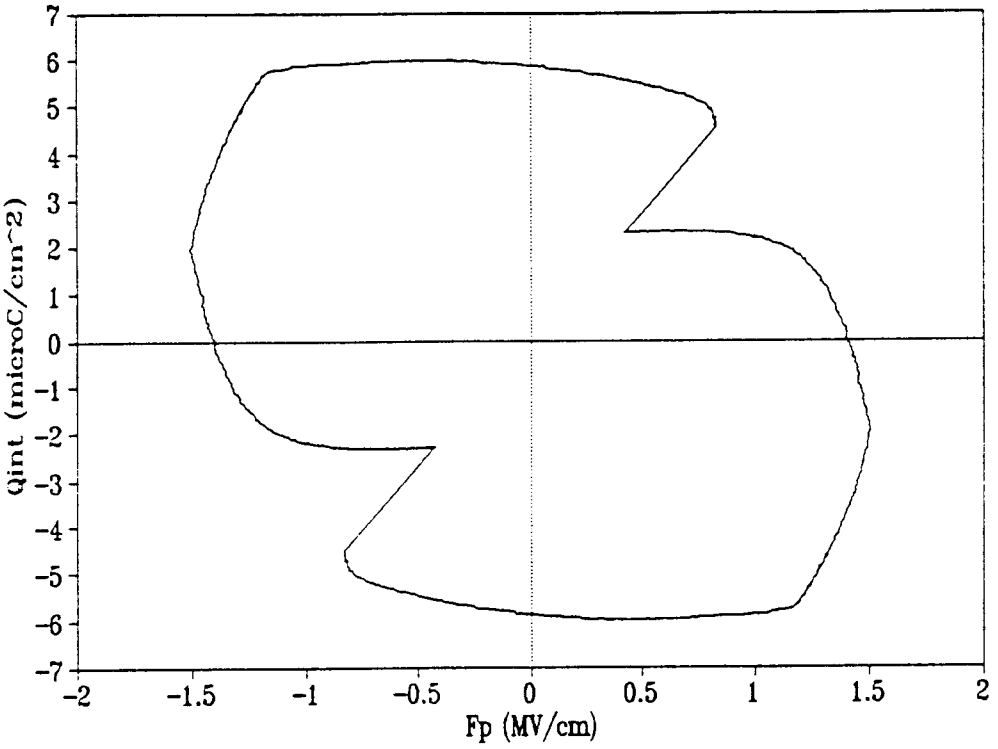

Figure 4-1. Q-F_p plot of an $AlInN_2$:Eu_2O_3 ACTFEL device.

4.2.2 $MgSiN_2$:Eu_2O_3

The $MgSiN_2$:Eu_2O_3 phosphor is studied next. This phosphor thin film has the following electrical properties: dielectric constant of 14, resistivity of 1.1×10^{13} ohm-cm, and breakdown field of 5.08 MV/cm. A $MgSiN_2$:Eu_2O_3 ACTFEL device is then fabricated and tested. The device exhibits no conduction nor luminescence at the maximum voltage of 293 volts or the corresponding phosphor field of 4.9 MV/cm.

4.2.3 $ZnSiN_2:Eu_2O_3$

The $ZnSiN_2:Eu_2O_3$ phosphor thin film is very non-transparent and conductive; therefore this material cannot be used as an ACTFEL phosphor.

4.2.4 $CaSiN_2:Eu_2O_3$

Based on photoluminescence (PL) results obtained with $MgSiN_2$, which exhibits blue PL with 40% quantum efficiency when doped with Eu, $CaSiN_2:Eu_2O_3$ is believed to be a good ACTFEL phosphor candidate material. However, this material still has not been evaluated because it was not possible to form a target using the cold press available. A different pressing technique (e.g. a hot press) is needed to press this material.

A summary of the electrical properties and ACTFEL device performance for $AlInN_2:Eu_2O_3$, $MgSiN_2:Eu_2O_3$, $ZnSiN_2:Eu_2O_3$, and $CaSiN_2:Eu_2O_3$ phosphors is given in Table 4-3.

4.2.5 $Mg(Si_{0.5}Ge_{0.5})N_2:Eu_2O_3$

Since it has been shown that a $MgGeN_2:Eu_2O_3$ ACTFEL device exhibits red electroluminescence at low voltages [2] and that a $MgSiN_2:Eu_2O_3$ ACTFEL device exhibits a very high breakdown field, the next phosphor uses a combination of silicon and germanium in order to lower the breakdown field. This new phosphor is $Mg(Si_{0.5}Ge_{0.5})N_2:Eu_2O_3$. This material thin film has the following electical properties: dielectric constant of 14.2, resistivity of 8.51×10^{12} ohm-cm, and breakdown field of 3.37 MV/cm. Notice, that

by replacing half of the silicon in $MgSiN_2:Eu_2O_3$ with Ge, the breakdown field is reduced from 5.08 MV/cm to 3.37 MV/cm; unforfunately, this is still too high for ACTFEL applications.

A $Mg(Si_{0.5}Ge_{0.5})N_2:Eu_2O_3$ ACTFEL device is fabricated and tested. The device shows very little conduction charge (about 0.6 microC/cm^2) and no luminescence at 280 volts. This is probably due to the high breakdown field.

Phosphor	ε	ρ (Ωcm)	F_{BR} (MV/cm)	Q_{cond} ($\mu C/cm^2$)	Comment
AlInN2:Eu2O3	12.5	2.2×10^{9}	1.5	8	Low field conduction Too leaky
MgSiN2:Eu2O3	14	1.1×10^{13}	5.0	0	F_{BR} too high
ZnSiN2:Eu2O3	-	low	low	-	Non-transparent
CaSiN2:Eu2O3	-	-	-	-	Cannot press target

Table 4-3. Summary of the properties of several novel phosphors.

4.2.6 $(Mg_{0.8}Zn_{0.2})SiN_2:EuF_3$

Since $MgSiN_2:Eu_2O_3$ has very high a breakdown field and $ZnSiN_2:Eu_2O_3$ has a very low breakdown field, by combining these two materials, the breakdown field may be controlled. The next target uses 80% magnesium and 20% zinc since a $ZnSiN_2:Eu_2O_3$ thin film is believed to be very conductive (i.e. has a very low breakdown field). The phosphor film deposited from this target is

$(Mg_{0.8}Zn_{0.2})SiN_2:EuF_3$ and it has the following electrical properties: dielectric constant of 10.9, resistivity of $8x10^{12}$ ohm-cm, and breakdown field of 2.5 MV/cm. Notice that the breakdown field is about half that of the $MgSiN_2:Eu_2O_3$ phosphor. Also, the film is very transparent.

The $(Mg_{0.8}Zn_{0.2})SiN_2:EuF_3$ ACTFEL device is fabricated using the structure shown in Fig. 3-1 but without a ZnS layer. Even though the measured breakdown field is quite low, no conduction charge is observed at 290 volts. This observation is presumably due to the small density of interface states or the fact that these interface states are very deep. To overcome this problem, another $(Mg_{0.8}Zn_{0.2})SiN_2:EuF_3$ ACTFEL device is fabricated using the structure shown in Fig. 3-1. For this device, conduction begins at approximately 200 volts. Dim blue luminescence was also observed at this voltage but the luminescence changes color to red at about 290 volts. The dim blue luminescence is attributed to the hot electron luminescence of the ZnS layer and the red luminescence is probably due to the impact excitation of Eu by electrons in the $(Mg_{0.8}Zn_{0.2})SiN_2:EuF_3$ layer, with subsequent radiative emission.

The $(Mg_{0.8}Zn_{0.2})SiN_2:EuF_3$ ACTFEL device using the ZnS charge injection layer is believed to operate as follows. At 200 volts, carriers are injected from the BTO-ZnS interface into the ZnS conduction band and are transported towards the phosphor. Due to the ZnS-phosphor conduction band discontinuity, carriers are trapped at the ZnS-phosphor interface. At a bias of approximately 290 volts,

when the band bending is sufficient that electrons are injected into the phosphor conduction band and impact excitation of Eu begins.

4.2.7 $(Mg_{0.6}Zn_{0.4})SiN_2:EuF_3$

Although the $(Mg_{0.8}Zn_{0.2})SiN_2:EuF_3$ ACTFEL device using the ZnS charge injection layer looks very promising, the voltage at which injection of charge from the ZnS-phosphor interface into the phosphor conduction band occurs is still very high. One way to reduce this voltage is by lowering the bandgap of the phosphor material. The bandgap can be reduced by lowering the breakdown field, because it is proportional to the breakdown field. The breakdown field of $(Mg_{0.8}Zn_{0.2})SiN_2:EuF_3$ film can be lowered by decreasing the Mg concentration and increasing the Zn concentration. The new phosphor film is $(Mg_{0.6}Zn_{0.4})SiN_2:EuF_3$. Notice that Mg is reduced to 60% and Zn is increased to 40%. This new phosphor film has the following electrical properties: dielectric constant of 15, resistivity of $1.2x10^{13}$ ohm-cm, and breakdown field of 2 MV/cm.

A $(Mg_{0.6}Zn_{0.4})SiN_2:EuF_3$ ACTFEL device is fabricated using the structure shown in Fig. 3-1. Conduction starts at approximately 200 volts. Red luminescence is also observed at this voltage. At 275 volts, the conduction charge is 2.75 micro/cm^2 and the brightness is 0.045 fL.

The $(Mg_{0.6}Zn_{0.4})SiN_2:EuF_3$ ACTFEL device using the ZnS charge injection layer is believed to operate as follows. At 200 volts, electrons are injected from the ATO-ZnS interface into the ZnS conduction band and are transported toward the phosphor. Due to a

smaller ZnS-phosphor conduction band discontinuity, these electrons surmount this barrier and are injected into the phosphor conduction band.

A summary of the electrical properties and ACTFEL device performance for the $Mg(Si_{0.5}Ge_{0.5})N_2:Eu_2O_3$, $(Mg_{0.8}Zn_{0.2})SiN_2:EuF_3$, and $(Mg_{0.6}Zn_{0.4})SiN_2:EuF_3$ phosphors is given in Table 4-4.

Phosphor	ε	ρ (Ωcm)	F_{BR} (MV/cm)	Q_{cond} ($\mu C/cm^2$)	Comment
Mg(Si0.5Ge0.5)N2 Eu2O3	14.2	$8.5x10^{12}$	3.37	0.6	Small conduction charge. F_{BR} too high.
(Mg0.8Zn0.2)SiN2 EuF3	10.9	$8x10^{12}$	2.5	-	Red luminescence is observed at 290 volts.
(Mg0.6Zn0.4)SiN2 EuF3	11	$1.2x10^{13}$	2	2.75	Red luminescence is observed at 200 volts.

Table 4-4. Summary of the properties of several novel phosphors.

4.2.8 $(Mg_{0.5}Zn_{0.5})SiN_2:Tb_4O_7$

$(Mg_{0.5}Zn_{0.5})SiN_2:Tb_4O_7$ is investigated next. Notice that the ratio of Mg and Zn is altered to further lower the breakdown field and that the luminescent impurity is now terbium (Tb), which is expected to emit green luminescence. The $(Mg_{0.5}Zn_{0.5})SiN_2:Tb_4O_7$ ACTFEL device gives off bright green luminescence at 290 volts. This is the best ACTFEL device built to date; therefore, $(Mg_{0.5}Zn_{0.5})SiN_2:Tb_4O_7$ is

chosen to be characterized in more detail, as presented in the next section.

4.3 $(Mg_{0.5}Zn_{0.5})SiN_2:Tb_4O_7$ Thin Film and ACTFEL Device Characterization.

4.3.1 Thin Film Characterization

4.3.1.1 Electrical and Optical Measurements

The measured electrical and optical properties of the $(Mg_{0.5}Zn_{0.5})SiN_2:Tb_4O_7$ film are the resistivity, the dielectric constant, and the optical bandgap, E_o. In order to have a large voltage drop across the phosphor, the phosphor dielectric constant must be low compared to that of the insulator. Also, it is desired to have a phosphor film with high resistivity to minimize leakage current. In order to allow the maximum propagation of light from the phosphor to the viewer, the phosphor must be transparent. Finally, in order to minimize the ZnS-phosphor conduction band discontinuity, the phosphor bandgap should be close to that of ZnS.

Phosphor	ε	ρ (Ωcm)	F_{BR} (MV/cm)	Eo (eV)
(Mg0.5Zn0.5)SiN2 Tb4O7	11	1.4×10^{13}	2	4
ZnS:Mn	6.3	10^{12}	-	3.75

Table 4-5. Summary of the electrical and optical properties of $(Mg_{0.5}Zn_{0.5})SiN_2:Tb_4O_7$ and ZnS:Mn films.

Figure 4-2 shows a Tauc plot along with the measured absorption coefficient of a $(Mg_{0.5}Zn_{0.5})SiN_2:Tb_4O_7$ film. Two linear fits to the Tauc plot are illustrated in Fig. 4-2 which define thresholds of about 3.6 and 4 eV; it could be argued that either of these define the optical bandgap, E_O. Note that the absorption curve shows a peak a about 3.7 eV; this kind of peak structure is often due to optical transitions to or from deep level states in the bandgap. Thus, it would appear that the optical bandgap, E_O, is greater than 3.7 eV. Thus E_O is estimated to be approximately 4 eV, but it must be recognized that there are large error bars associated with this estimate.

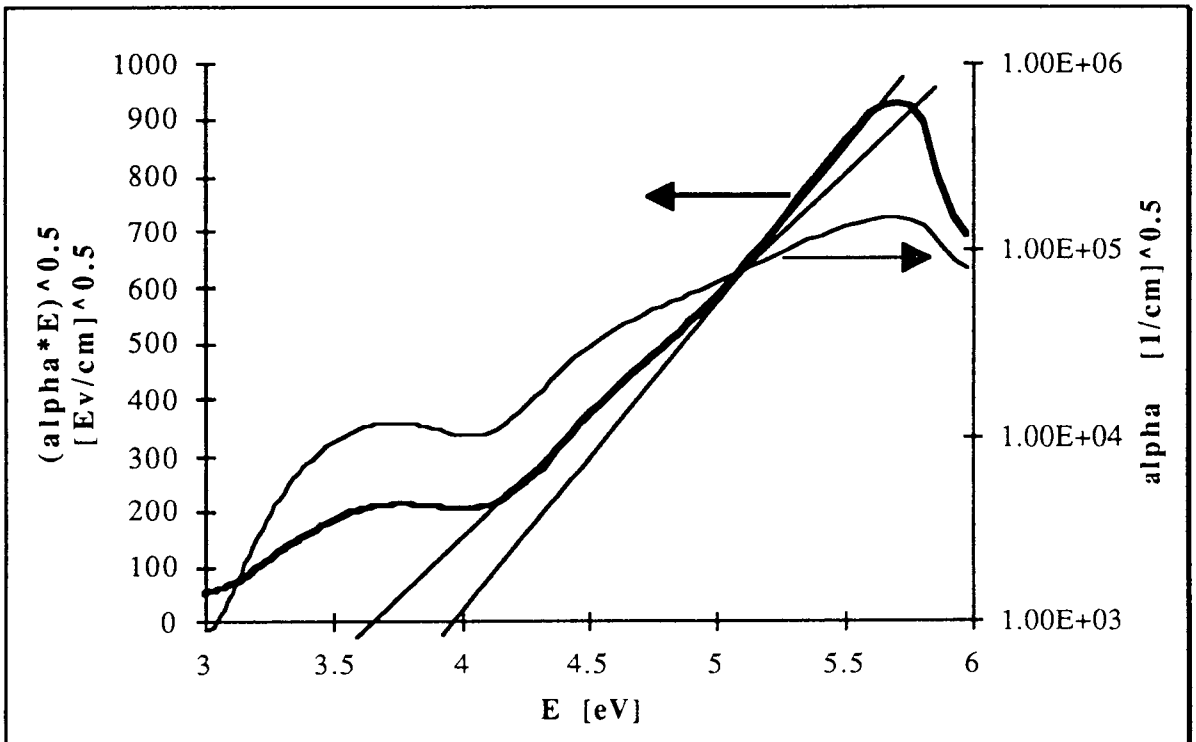

Figure 4-2. Tauc plot of a $(Mg_{0.5}Zn_{0.5})SiN_2:Tb_4O_7$ film.

A summary of the electrical and optical properties of $(Mg_{0.5}Zn_{0.5})SiN_2:Tb_4O_7$ and ZnS films is presented in Table 4-5. The dielectric constant of the $(Mg_{0.5}Zn_{0.5})SiN_2:Tb_4O_7$ film is higher that

that of ZnS:Mn. The resistivity is about 1 order of magnitude higher than than of ZnS:Mn. The bandgap is about the same as that of ZnS:Mn.

4.3.1.2 Structural Characterization

The x-ray diffraction spectrum for a $(Mg_{0.5}Zn_{0.5})SiN_2:Tb_4O_7$ film deposited onto a pre-deposited ITO glass is presented in Fig. 4-3. From the plot, it is seen that there are three main peaks. These peaks reside at 2-theta of 30.9, 35.7, and 51.3, which are attributed to the crystal structure of silicon nitride (Si_3N_4), magnesium silicon nitride ($MgSiN_2$), and zinc nitride (Zn_3N_2) respectively. From this result, it is concluded that there is some crystallization of the thin film as it is deposited onto the glass substrate at room temperature.

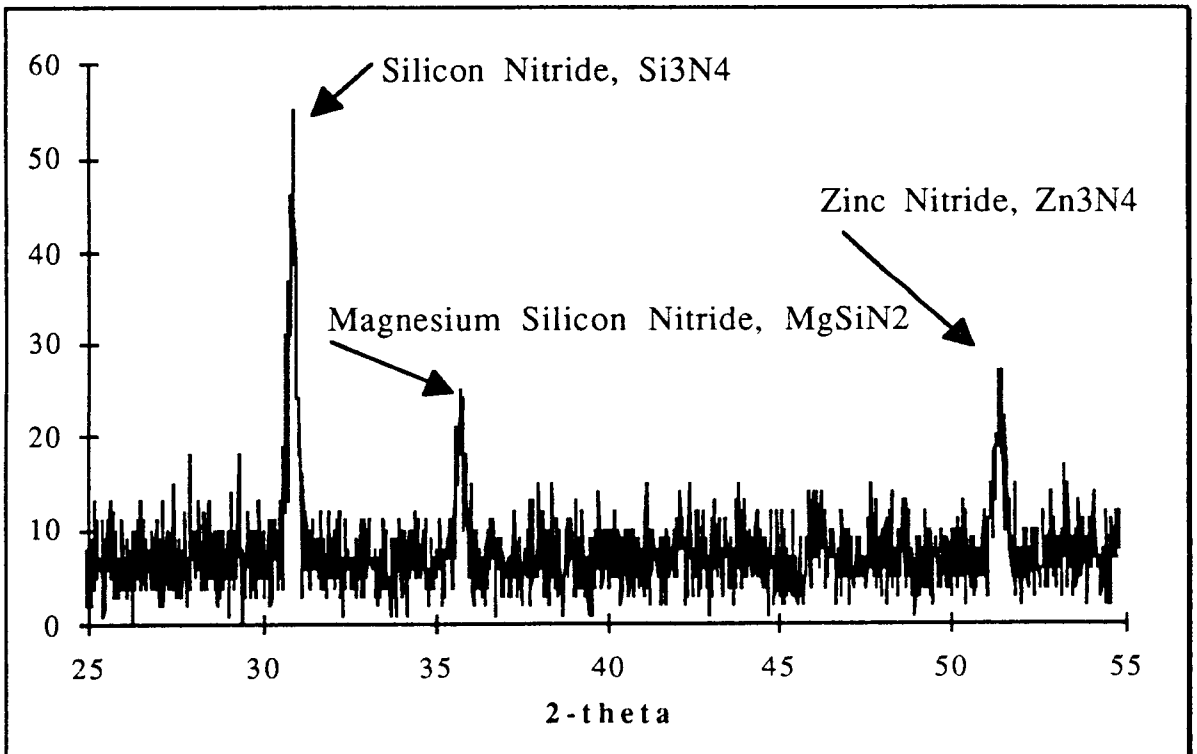

Figure 4-3. X-ray diffaction of a $(Mg_{0.5}Zn_{0.5})SiN_2:Tb_4O_7$ film.

X-ray diffraction results for films after post-deposition annealing at 500 C, 600 C, 650 C, and 700 C are similar to that of the as-deposited film. Thus, there is no sign of crystal structure enhancement due to post-deposition annealing.

4.3.2 ACTFEL Device Characterization

4.3.2.1 C-V, Q_a-V_a, and Q-F_p Measurements

A C-V plot taken at 280 volts is shown in Fig. 4-4. From this plot, the measured insulator capacitance (C_i) is 1.5 nF and the total capacitance (C_t) is 1.25 nF. The phosphor capacitance (C_p) is given by

$$C_p = \frac{C_i C_t}{C_i - C_t}, \qquad (4\text{-}1)$$

and, thus, it is equal to 7.5 nF.

Several assumptions are made in the above analysis. First, it is assumed that C_t and C_i can be accurately estimated from the C-V measurement. In fact, C_t can indeed be reliably assessed from the C-V measurement because below breakdown the total capacitance is simply a series combination of all of the capacitances of all of the layers in series. However, in general C_i will not be equal to C_i' estimated from a C-V measurement since this only occurs if a sufficient conduction current flows across the phosphor such that the phosphor capacitance can be considered to be entirely shunted. Note that this is very often not the case, particularly when electron injection into the phosphor is inhibited because of the existence of a

barrier at the injector-phosphor interface. Therefore, a more general treatment is required, as presented next.

An equivalent circuit for an ACTFEL device with a charge injection layer prior to breakdown is shown in Fig. 4-5a. Notice that C_z is the capacitance of the ZnS charge injection layer and C_p is the

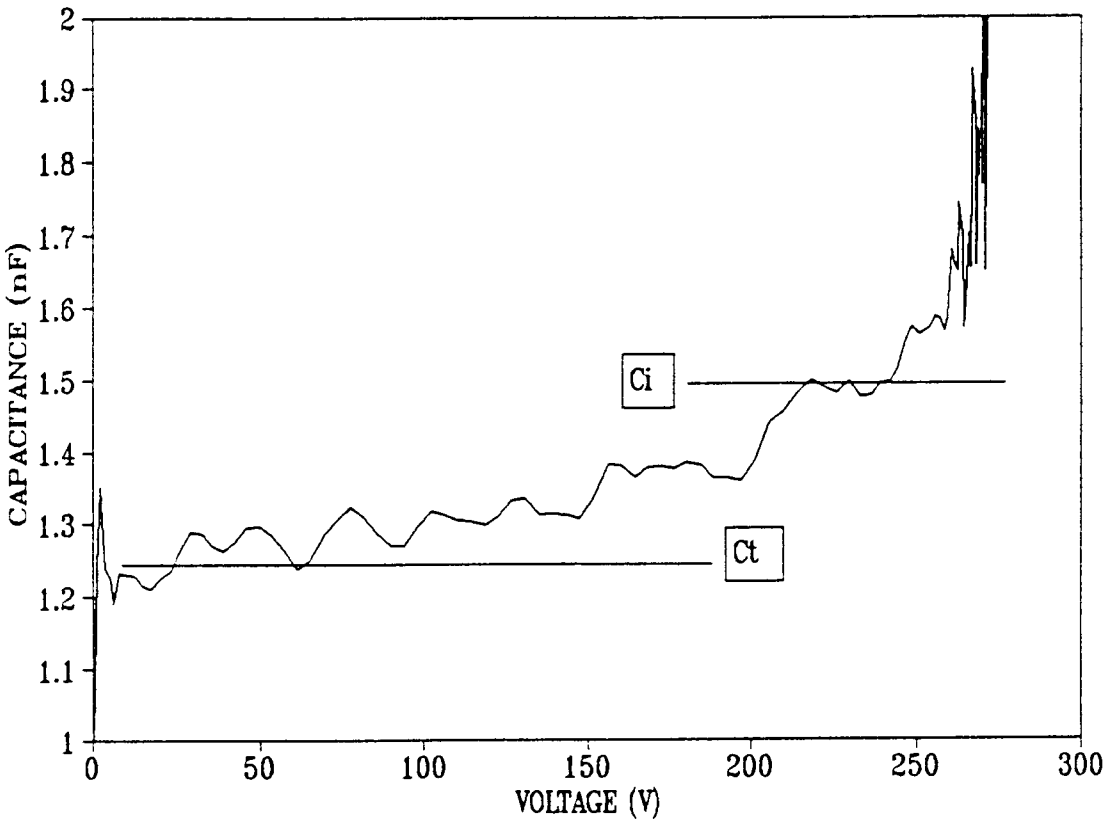

Figure 4-4. C-V plot of a $(Mg_{0.5}Zn_{0.5})SiN_2$:Tb_4O_7 ACTFEL device.

capacitance of the phosphor layer. Figure 4-5b shows an equivalent circuit for the ACTFEL device with a charge injection layer in which the phosphor layer breakdown is not complete (i.e. an insufficient current flows through the phosphor for it to be shunted out of the

circuit). C_{pz} denotes the capacitance due to the fact that the phosphor breakdown is incomplete.

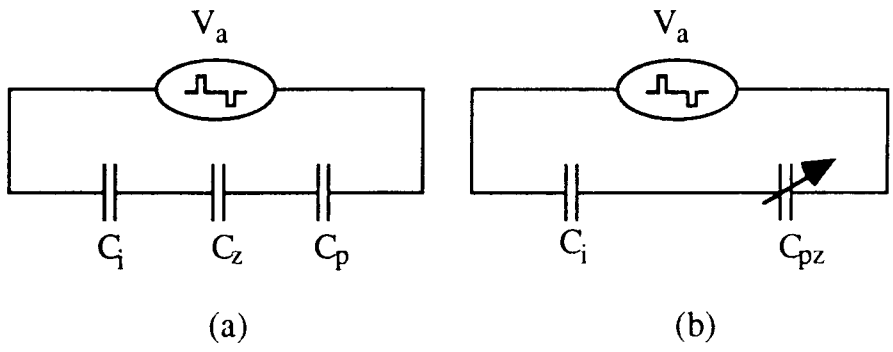

Figure 4-5a. An equivalent circuit of an ACTFEL device with a ZnS injector layer, prior to breakdown.

Figure 4-5b. An equivalent circuit of an ACTFEL device with an injector layer in which the phosphor layer not fully breaking down.

For the subsequent analysis, capacitances will be designated as unprimed, primed, or double primed (eg. C_i, C_i', or C_i'') which denotes the respective actual capacitance, capacitance estimated from C-V measurement, or capacitance estimated from the equation

$$C = \frac{\varepsilon A}{d} \qquad (4\text{-}2)$$

where ε, A, and d are the measured or expected values for the dielectric constant, area, and thickness, respectively.

First, as discussed previously, it is assumed that $C_i = C_i''$. Next, C_{pz} is obtained from:

$$\frac{1}{C_{pz}} = \frac{1}{C_i'} - \frac{1}{C_i}. \qquad (4\text{-}3)$$

C_{pz} is interpreted as the phosphor capacitance when the breakdown is incomplete. If it is assumed that the ZnS charge injection layer is fully broken down and that C_p can be accurately estimated as C_p'', then the magnitude of C_{pz} is bounded as follows:

$$C_p \leq C_{pz} \leq \infty. \qquad (4\text{-}4)$$

$C_{pz}=\infty$ when the phosphor breakdown is complete whereas $C_{pz}=C_p$ when no conduction current flows through the phosphor layer. Thus, the magnitude of C_{pz} may be used to establish the extent of breakdown of the phosphor.

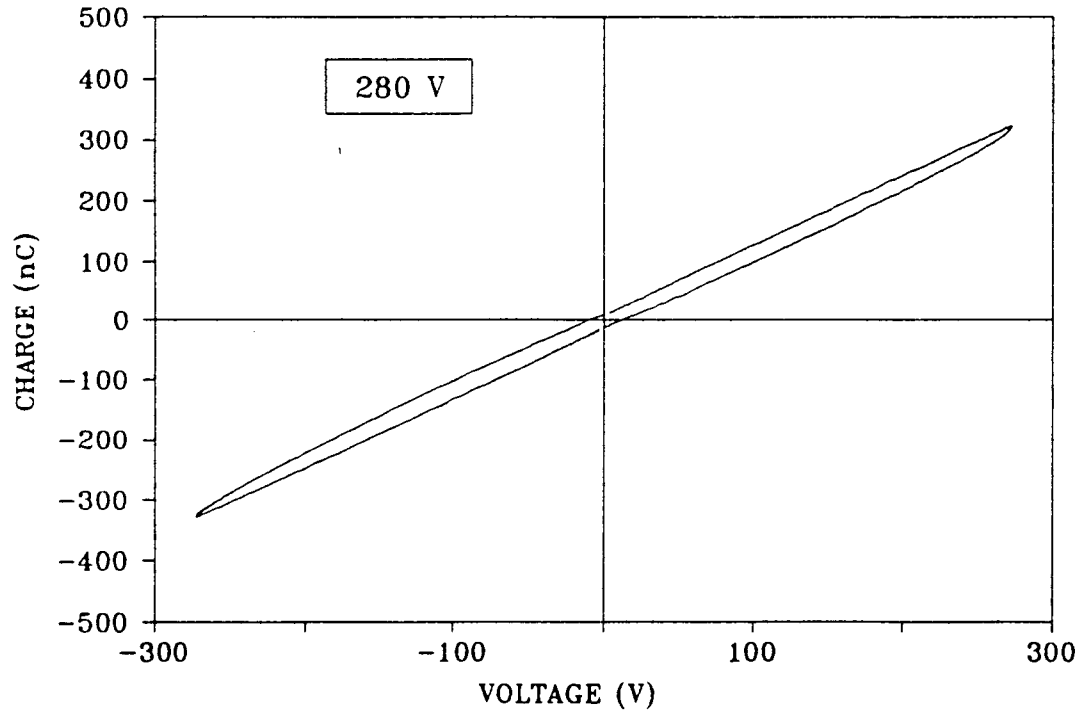

Figure 4-6. Q_a-V_a plot of a $(Mg_{0.5}Zn_{0.5})SiN_2$:Tb_4O_7 ACTFEL device.

This formulation is now employed to assess the $(Mg_{0.5}Zn_{0.5})SiN_2:Tb_4O_7$ ACTFEL device of Fig. 4-4. Using the new notation, $C_i=C_i''=6.23$ nF and $C_p=C_p''=1.82$ nF from $\varepsilon_i=18$, $\varepsilon_p=11$, $d_i=2200$ angstrom, $d_p=4600$ angstrom, and $A=0.086$ cm^2. Inserting $C_i=6.23$ nF and $C_i'=1.5$ nF in Eqn. 4-3 yields $C_{pz}=1.97$ nF. Comparing C_{pz} to C_p, it is seen that C_{pz} is quite close to C_p; therefore it can be

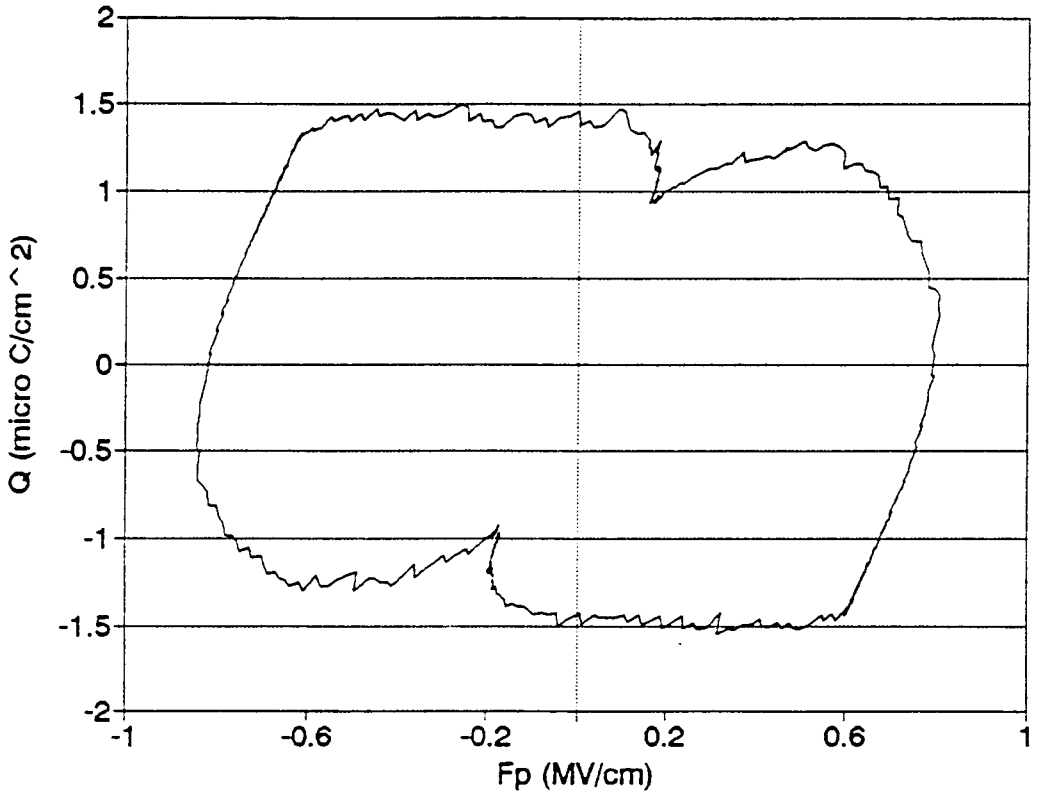

Figure 4-7. Q-F_p plot of a $(Mg_{0.5}Zn_{0.5})SiN_2:Tb_4O_7$ ACTFEL device.

concluded that the $(Mg_{0.5}Zn_{0.5})SiN_2:Tb_4O_7$ phosphor is only weakly broken down.

A Q_a-V_a plot is presented in Fig. 4-6 for V_a 280 volts. It is very difficult to determine the turn-on voltage and the amount of conduction charge from this plot. Nevertheless, this plot shows that

the displacement charge is much larger than the conduction charge. This is presumably due to the fact that the phosphor layer does not break down totally.

A Q-F_p plot at 280 volts is shown in Fig. 4-7. This plot is calculated employing C_i'=1.5 nF and C_p'=7.5 nF obtained from the C-V plot. The plot shows that about 2.8 microC/cm^2 of charge conducts across the device. Note that due to the fact that the $(Mg_{0.5}Zn_{0.5})SiN_2$:Tb_4O_7 layer does not fully break down, only a portion of this charge is actually transported across the phosphor layer while the rest is trapped at the ZnS-phosphor interface. Also, Fig. 4-7 shows that the device does not appear to exhibit field-clamping.

Calculation of the phosphor electric field is as follow. From the Q-F_p plot of Fig. 4-7, the average phosphor field rises to a maximum value of about 0.8 MV/cm. At this field, the sum (V_s) of the voltage drop across the ZnS layer and the voltage drop across the $(Mg_{0.5}Zn_{0.5})SiN_2$:Tb_4O_7 layer is

$$V_s=0.8x10^6*(d_p+d_z), \qquad (4-5)$$

and, thus, it is equal to 49 V. Assuming that the field across the ZnS layer is clamped at 1.5 MV/cm, the voltage drop across the ZnS layer is 4.5 V; the remainder of V_S (i.e. 49-4.5=44.5 V) drops across the phosphor layer (V_{ps}). Also, the insulator voltage, i.e. the voltage drop across C_i and C_{pz}, is 231 V. The voltage drop across C_{pz} (i.e. the residual phosphor capacitance due to the fact that breakdown in the phosphor is not complete) is given by

$$V_{pz} = \frac{C_i}{C_i + C_{pz}} 231, \qquad (4\text{-}3)$$

and, thus, it is equal to 175.5 V. The phosphor voltage (V_p) is the sum of V_{ps} and V_{pz} which is equal to 220 V. The phosphor field (F_p) is, therefore, given by

$$F_p = \frac{V_p}{d_p} \qquad (4\text{-}8)$$

or 4.8 MV/cm. This field is about three times higher than the steady-state field of a ZnS:Mn ACTFEL device.

4.3.2.2 Electroluminescence Spectrum Measurement

Electroluminescence from the $(Mg_{0.5}Zn_{0.5})SiN_2$:Tb_4O_7 ACTFEL device is visually observable at an applied voltage of 280 V. The color of the electroluminescence is green. Usually, Tb-doped phosphors exhibit electroluminescence with a spectrum composed sharp peaks at a wavelength of approximately 540 nm. In order to establish whether Tb is indeed responsible for the electroluminescence, the emission spectrum of this device is measured.

An electroluminescence spectrum of the $(Mg_{0.5}Zn_{0.5})SiN_2$:Tb_4O_7 ACTFEL device taken at 280 V is shown in Fig. 4-8. Also, an electroluminescence spectrum of the ZnS:TbF_3 phosphor is shown in Fig 4-9. Both phosphors possess similar peaks through out the spectrum. The Tb peaks in the $(Mg_{0.5}Zn_{0.5})SiN_2$:Tb_4O_7 spectrum are

assigned by comparing the electroluminescence spectrum to that of $ZnS:TbF_3$.

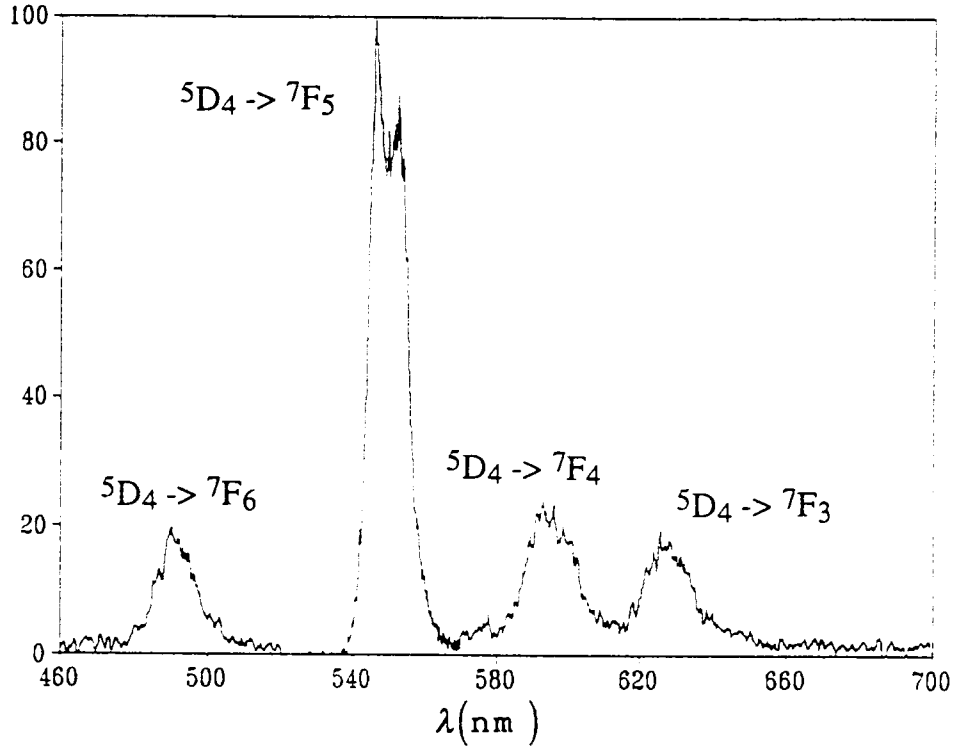

Figure 4-8. Electroluminescence spectrum of a $(Mg_{0.5}Zn_{0.5})SiN_2:Tb_4O_7$ ACTFEL device.

4.3.2.3 B-V Measurement

A (B-V) curve for the $(Mg_{0.5}Zn_{0.5})SiN_2:Tb_4O_7$ ACTFEL device is shown in Fig. 4-10. The maximun brightness is about 0.53 foot-lambert (fL) at a voltage of 308 V and a frequency of 1000 Hz; this is a very low brightness. Commercial green phosphors require a brightness of about 20 fL at the frequency of 60 Hz. The low brightness could be caused by insufficient conduction charge across

the phosphor. Also, although x-ray diffraction analysis indicates that the existence of some crystallinity, the relatively poor crystallinity of present devices undoubtedly leads to inefficient heating of the transported electrons. Another possible reason for the poor performance of the present $(Mg_{0.5}Zn_{0.5})SiN_2:Tb_4O_7$ ACTFEL device is due to concentration quenching of Tb atoms, although this seems

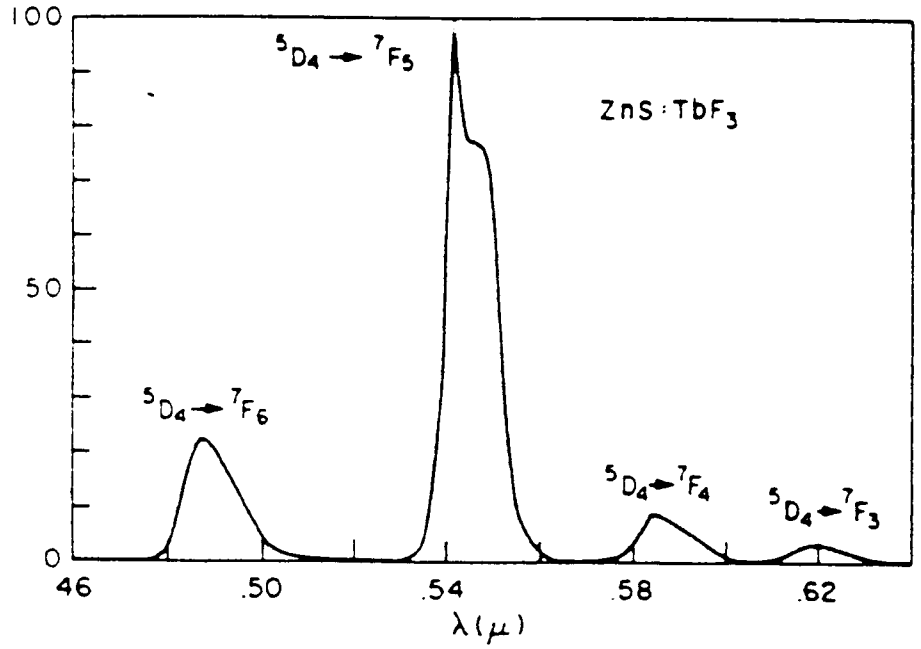

Figure 4-9. Electroluminescence spectrum of a ZnS:TbF3 phosphor duplicated from reference 21.

unlikely since a concentration of 1% is commonly used in ZnS:TbF3 ACTFEL devices, which are very efficient in emitting green light. Although the present device is quite dim, the results obtained herein are considered encouraging at the early stage of development of this material.

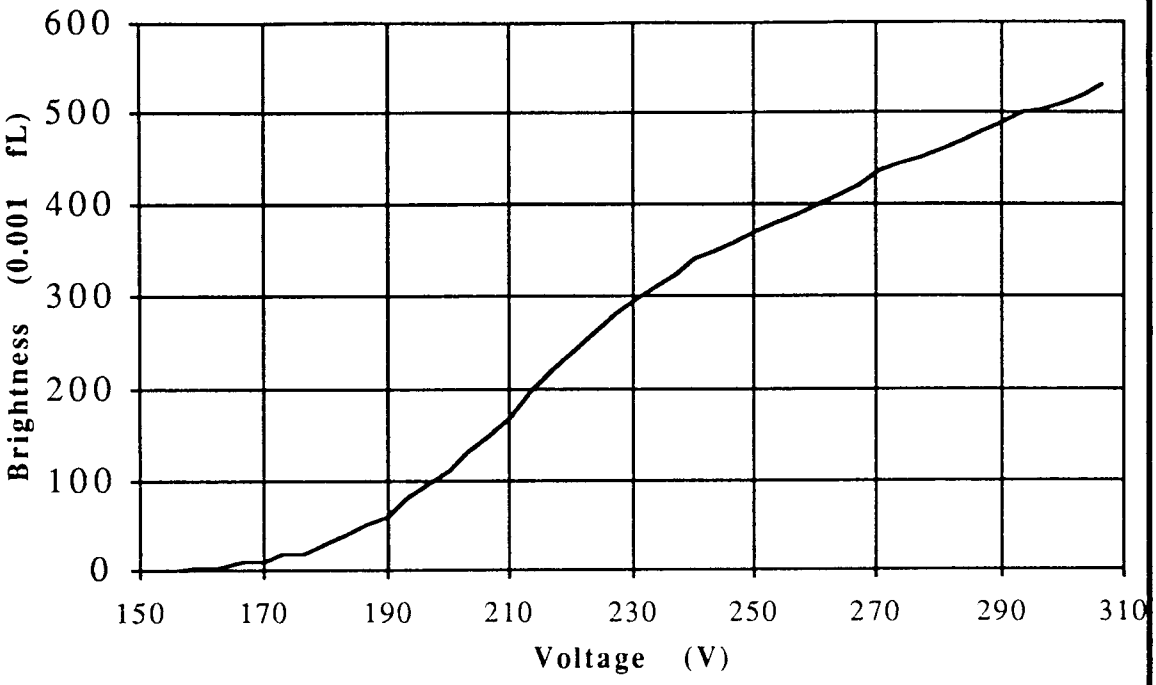

Figure 4-10. B-V plot of a $(Mg_{0.5}Zn_{0.5})SiN_2:Tb_4O_7$ ACTFEL device.

Chapter 5 - Conclusions and Recommendations for Future Work

5.1 Conclusions

This thesis describes a research program with the long-term goal of exploring the potential of new phosphor materials for alternating-current thin-film electroluminescence applications.

The main accomplishment of this thesis is the fabrication of an ACTFEL device employing $(Mg_{0.5}Zn_{0.5})SiN_2$:Tb_4O_7 as the phosphor which emits green electroluminescence. A $(Mg_{0.5}Zn_{0.5})SiN_2$:Tb_4O_7 ACTFEL device is fabricated with an additional ZnS charge injection layer between the insulator and phosphor layer, because $(Mg_{0.5}Zn_{0.5})SiN_2$:Tb_4O_7 either has a small density of interface states or these interface states are very deep. From Q-F_p analysis, it is evident that charge is conducted across the phosphor, field-clamping does not occur in this device, and the steady-state phosphor electric field is approximately 4.8 MV/cm. Green electroluminescence is observed but it is quite dim; the maximum brightness is 0.53 fL at a voltage of 308 V and a frequency of 1000 Hz. The green electroluminescence is an indication that Tb with a valence of +3 is present in $(Mg_{0.5}Zn_{0.5})SiN_2$:Tb_4O_7. The $(Mg_{0.5}Zn_{0.5})SiN_2$:Tb_4O_7 thin film deposited is found to be polycrystalline with a dielectric constant, resistivity, breakdown field, and optical bandgap of 11, 1.4×10^{13} ohm-cm, 2 MV/cm, and 4 eV, respectively. $(Mg_{0.5}Zn_{0.5})SiN_2$:Tb_4O_7 films subject to post-deposition annealing up

to the temperature of 700 C show no improvement in their crystal structure.

A $(Mg_{0.6}Zn_{0.4})SiN_2:EuF_3$ ACTFEL device with a ZnS charge injection layer is also fabricated. Red electroluminescence is observed but it is very dim; the maximum brightness is 0.045 fL at a voltage of 308 V and a frequency of 1000 Hz. The red elctroluminescence is attributed to impact excitation of Eu and subsequent radiative emission; also, it is an indication that Eu with the valence of +3 is presented in $(Mg_{0.6}Zn_{0.4})SiN_2$. The $(Mg_{0.6}Zn_{0.4})SiN_2:EuF_3$ thin film has the following electrical properties: dielectric constant of 11, resistivity of $1.2x10^{13}$ ohm-cm, and breakdown field of 2 MV/cm.

5.2 Recommendations for Future Work

Several areas of research should be explored in order to improve the quality of the $(Mg_{0.5}Zn_{0.5})SiN_2:Tb_4O_7$ thin films and, hence, improve the brightness of an ACTFEL device employing this phosphor film.

1. The dim electroluminescence is attributed to the small amount of conduction charge which flows across the phosphor. The conduction charge can be increased by lowering the breakdown field of the $(Mg_{0.5}Zn_{0.5})SiN_2$ thin film, which can be accomplished by changing the ratio of Mg to Zn in the film.

2. Attempts should be made to improve the crystalline quality of the $(Mg_{0.5}Zn_{0.5})SiN_2:Tb_4O_7$ film. This could be accomplished by post-deposition annealing of the film using rapid thermal annealing (RTA) or depositing the phosphor film at an elevated temperature.

3. Employ different luminescence impurities, eg. Thulium, for blue luminescence and samarium, for red luminescence.

4. A different pressing technique (e.g. a hot press) should be employed to form the $CaSiN_2:Eu_2O_3$ target so that this material can be evaluated.

Bibliography

1. G.K Gaido, G.P. Dubrovskii, and A.M. Zykov, "Photoluminescence of $MgSiN_2$ Activated by Europium", Inorganic Materials, pp. 485-487. (translated from Izvestiya Academii Nauk SSSR, 10 (3), pp. 564-566, 1974.)
2. M. Ang, Oregon State University, M.S. Thesis, 1992.
3. F. Kido, N. Matsuda, H. Yoshikawa, and M. Tamatani, "Thin Film Electroluminescence Device with Zn Concentration Gradient", United States Patent # 5,029,320.
4. G. Destriau, J. Chem. Phys., 33 (1936) 587.
5. T. Inoguchi, M. Takeda, Y. Kakihara, Y. Nakata, and M. Yoshida, SID 74 Digest, (1974) 84.
6. R.T. Tuenge, and J. Kane, "Bright Red EL Using a Thin-Film Filter", SID 91 Digest, (1991) 279
7. G. Harkonen and H. Hardonen, "Green Emitting TFEL device Grown by ALE", SID International Symposium Digest, 13.1, 1990.
8. V. Shander, S. Tanaka, M. Shiike, H. Deguchi, H. Kobayashi, and H. Sasakura, "Electroluminescence in Thin-Film CaS:Ce", Appl. Phys. Lett. 45 (906), 1984.
9. SID International Symposium, Planar Systems vendor display, 1993.
10. S. Tanaka, V. Shander, M. Shiiki, H. Deguchi and H. Kobayashi, Digestt 1985 SID Int'l Symp., 218, 1985.
11. A.A. Douglas and J.F. Wager, "Electrical Characterization and Modeling of ZnS:Mn ACTFEL Devices with Various Pulse Waveforms", SID 92 Digest, (1992) 356.

12. G.O. Mueller, R. Mach, B. Selle, and G. Shulz, "Measuring on Thin-Film Electroluminescent Devices", Phys. Stat. Sol. (a) 110, 657, 1988.

13. R. Mach and G.O. Mueller, "Physical Comcepts of High Field, Thin-Film Electroluminescent Devices", Phys. Stat. Sol. (a), 69 (11), 1982.

14. J.D. Davidson, J.F. Wager, R.I. Khormaei, C.N. King, and R. Williams, "Electrical Characterization and Modeling of Alternating-Current Thin-Film Electroluminescent Devices", IEEE Transcations on Electron Devices, Vol. 39, No. 5, pp. 1122-1128, 1992.

15. A.A. Douglas and J.F. Wager, "Electrical Characterization and Modeling of ZnS:Mn ACTFEL Devices with Various Pulse Waveforms", SID 92 Digest, 19.5, 1992.

16. E. Bringuier, "Charge Transfer in ZnS-type Electroluminescence", J. Appl. Phys., 66 (3), pp.1314-1325, 1 August 1989.

17. J.D. Davidson, J.F. Wager, R.I. Khormaei, C.N. King, and R. Williams, "Electrical Characterization and Modeling of Alternating-Current Thin-Film Electroluminescent Devices", IEEE Transactions on Electron Devices, 39 (5), pp. 1122-1128, May 1992.

18. A. Abu-Dayah, S. Kibayashi, and J.F. Wager, "Internal Charge-Phosphor Field Characteristics of Alternating-Current Thin-Film electroluminescent Devices",

19. A.A. Douglas, Oregon State University, M.S. Thesis, 1993.

20. N.F. Mott and E.A. Davis, "Electronic Processes in Non-Crystaline Materials", Clarendon Press, Oxford, 1979.

21. E.W Chase, R.T. Hepplewhite, D.C. Krupka, and D. Kahng, "Electroluminescence of ZnS Lumocen Devices Containing Rare-Earth and Transition-Metal Flourides", J. Appl. Phys., 40 (6), pp. 2512-2519, May 1969.